


Establishment and Application of a Novel *In Vitro* Model of Microglial Activation in Traumatic Brain Injury

 Ning Liu,^{1,3} Yadan Li,¹ Yinghua Jiang,¹ Samuel Shi,¹ Aim Niamnud,¹ Sammy J. Vodovoz,¹ Prasad V.G. Katakam,^{1,2,3} Charles Vidoudez,⁴ Aaron S. Dumont,¹ and Xiaoying Wang^{1,3}

¹Clinical Neuroscience Research Center, Department of Neurosurgery and Neurology, Tulane University School of Medicine, New Orleans, Louisiana 70122, ²Department of Pharmacology, Tulane University School of Medicine, New Orleans, Louisiana, 70122, ³Neuroscience Program, Tulane Brain Institute, Tulane University, New Orleans, Louisiana, 70122, and ⁴Harvard Center for Mass Spectrometry, Harvard University, Cambridge, Massachusetts 02138

Mechanical impact-induced primary injury after traumatic brain injury (TBI) leads to acute microglial pro-inflammatory activation and consequently mediates neurodegeneration, which is a major secondary brain injury mechanism. However, the detailed pathologic cascades have not been fully elucidated, partially because of the pathologic complexity in animal TBI models. Although there are several *in vitro* TBI models, none of them closely mimic post-TBI microglial activation. In the present study, we aimed to establish an *in vitro* TBI model, specifically reconstituting the pro-inflammatory activation and associated neurodegeneration following TBI. We proposed three sets of experiments. First, we established a needle scratch injured neuron-induced microglial activation and neurodegeneration *in vitro* model of TBI. Second, we compared microglial pro-inflammatory cytokines profiles between the *in vitro* TBI model and TBI in male mice. Additionally, we validated the role of injured neurons-derived damage-associated molecular patterns in amplifying microglial pro-inflammatory pathways using the *in vitro* TBI model. Third, we applied the *in vitro* model for the first time to characterize the cellular metabolic profile of needle scratch injured-neuron-activated microglia, and define the role of metabolic reprogramming in mediating pro-inflammatory microglial activation and mediated neurodegeneration. Our results showed that we successfully established a novel *in vitro* TBI model, which closely mimics primary neuronal injury-triggered microglial pro-inflammatory activation and mediated neurodegeneration after TBI. This *in vitro* model provides an advanced and highly translational platform for dissecting interactions in the pathologic processes of neuronal injury-microglial activation-neuronal degeneration cascade, and elucidating the detailed underlying cellular and molecular insights after TBI.

Key words: *in vitro* model; metabolic reprogramming; microglia and neuron coculture; microglial pro-inflammatory activation; neuronal injury; traumatic brain injury

Significance Statement

Microglial activation is a key component of acute neuroinflammation that leads to neurodegeneration and long-term neurologic outcome deficits after TBI. However, it is not feasible to truly dissect primary neuronal injury-induced microglia activation, and consequently mediated neurodegeneration *in vivo*. Furthermore, there is currently lacking of *in vitro* TBI models closely mimicking the TBI primary injury-mediated microglial activation. In this study, we successfully established and validated a novel *in vitro* TBI model of microglial activation, and for the first time, characterized the cellular metabolic profile of microglia in this model. This novel microglial activation *in vitro* TBI model will help in elucidating microglial inflammatory activation and consequently associated neurodegeneration after TBI.

Received June 20, 2022; revised Nov. 8, 2022; accepted Nov. 17, 2022.

Author contributions: N.L., P.V.G.K., A.S.D., and X.W. designed research; N.L., Y.L., Y.J., S.S., A.N., S.J.V., and C.V. performed research; N.L., Y.L., and Y.J. analyzed data; N.L. wrote the first draft of the paper; N.L. and X.W. wrote the paper; Y.L., S.S., A.S.D., and X.W. edited the paper.

This work was supported in part by the National Institutes of Health Grants R01 NS092085-01 and R01 NS126503-01A1 to X.W., and AG074489 (NIA) and NS114286 (NINDS) to P.V.G.K.

The authors declare no competing financial interests.

Correspondence should be addressed to Ning Liu at nliu3@tulane.edu or Xiaoying Wang at xwang51@tulane.edu.

<https://doi.org/10.1523/JNEUROSCI.1539-22.2022>

Copyright © 2023 the authors

Introduction

Traumatic brain injury (TBI) is a devastating brain disorder and one of the leading causes of death and disability worldwide (Rozenbeek et al., 2013). However, there are currently no clinically effective pharmacologic therapies for TBI (Cox, 2018). The translational barrier is in part because of a lack of understanding in how TBI leads to neurodegeneration and other long-term impairments (Donat et al., 2017). The primary mechanical injury of TBI initiates multiple cell death processes, starting with cell

death of neurons, the most vulnerable cells in the brain, and progressing to various secondary brain damage mechanisms, particularly acute neuroinflammation (Schimmel et al., 2017). It is well demonstrated that microglial activation plays a crucial role in TBI-induced neuroinflammation (Donat et al., 2017; Witcher et al., 2021). Microglia are the brain resident immune cells and are activated rapidly by the potent inflammatory stimuli from the primary damaged neurons-released danger-associated molecular patterns (DAMPs) (Jassam et al., 2017). Consequently, the activated microglia release noxious substances, including pro-inflammatory cytokines, ROS, nitrogen species, and excitatory neurotransmitters, which cause subsequent neurodegeneration and exacerbate secondary brain damage (Alam et al., 2020; Isakharov and Butler, 2020). Therefore, targeting the early pro-inflammatory activation of microglia to inhibit secondary damage after TBI has been proposed as a therapeutic strategy (Henry et al., 2020; Bray et al., 2022). However, detailed underlying molecular mechanisms remain poorly understood, partially because of the complex and interactive multiple pathogenic/pathologic factors involved (Simon et al., 2017). Utilization of a simple *in vitro* culture TBI model is one of the common experimental approaches to dissect specific pathogenic/pathologic factors or pathways of specific cell types or between cells (Wu et al., 2021).

In vitro models have been recognized as necessary approaches to investigate the complex physiological and pathophysiological mechanisms after TBI (Xiong et al., 2013). However, *in vitro* TBI modeling approaches that are capable of mimicking the pathophysiological mechanisms underlying post-TBI microglial activation-mediated neurodegeneration are still lacking. A recent systematic review paper has summarized that stretch, blast, compression, scratch, shear, and fluid percussion injury are the most commonly used mechanical force in *in vitro* models of TBI (Wu et al., 2021). Among these mechanical injuries, the needle scratch or transection has been proposed to study secondary injury mechanisms, including glial activation, and is a representative model of penetrating (open-head) brain injuries (Morrison et al., 2011; Kumaria, 2017). Therefore, in this study, the needle scratch of neurons is used to mimic the primary neuronal injury of TBI. Considering that injured neuronal-released factors are the major stimulators responsible for the early microglial activation (Jassam et al., 2017), it is of significance to establish the neuron-microglia coculture system to investigate the neuronal injury-induced microglial activation, and the activation-mediated neurodegeneration *in vitro*.

In this study, we newly developed and validated an *in vitro* TBI model of microglial activation, in which: (1) neurons were first subjected to needle-scratch neuronal injury; (2) injured neurons and microglia were cocultured in monolayers of the different chambers of the coculture system to activate microglia; and (3) reactive microglia were further used to model neurotoxicity with naive neurons. We also applied this *in vitro* TBI model to validate and elucidate the role of two injured DAMPs (Wofford et al., 2019), including ATP and HMGB1, in triggering pro-inflammatory pathways that were well defined in microglia of TBI, and compare the pro-inflammatory profile of activated microglia between this *in vitro* TBI model and *in vivo* TBI mouse model. Moreover, for the first time, we characterize the metabolic profile of activated microglia in this *in vitro* model of TBI using comprehensive cellular metabolic analysis approaches. Moreover, by using this *in vitro* model of TBI, we defined and elucidated the roles of glycolysis in

controlling post-TBI microglial activation and associated neurodegeneration. We believe this *in vitro* TBI model provides a powerful tool to investigate the underlying cellular and molecular mechanisms of pro-inflammatory microglial activation and its associated neurodegeneration following TBI.

Materials and Methods

Ethics approval and consent to participate

All animal experiments were conducted following a protocol approved by The Institutional Animal Care and Use Committee of the Tulane University School of Medicine (#916, January 17, 2020) under the National Institutes of Health's *Guide for the care and use of laboratory animals*.

Culture of primary mouse neurons and microglia

WT C57/BL6J female and male mice (9 weeks old) were purchased from The Jackson Laboratory and used for breeding. All animal studies were performed according to the protocol approved by the Tulane University School of Medicine under the National Institutes of Health's *Guide for the care and use of laboratory animals*.

Primary mouse cortical neuronal cultures were prepared from the cortex of embryonic day 15 (E15) obtained from the pregnant C57BL/6 female mouse as we described previously (Yu et al., 2013; Liu et al., 2018). After removing the meninges, the cortical tissue was dissected and trypsinized with 0.05% trypsin-EDTA for 15 min at 37°C, followed by centrifugation at 1000 rpm for 5 min. Cell pellets were resuspended into DMEM plus 10% FBS and mechanically triturated. The mixed cells were filtered through a 40 μ m nylon mesh cell strainer (Fisher Scientific, catalog #501960596) and plated onto poly-D-lysine (Sigma)-coated plates with or without coverslips (round cover glass, #1.5 thickness, 10 mm, 100 pack, Fisher Scientific, catalog #NC1272767) at a density of 3×10^5 cells/ml and cultured in a humidified (5% CO₂, 37°C) incubator overnight. Following 16 h of incubation, the media was replaced with neurobasal complete medium (neuron basal A medium [NBA], supplemented with 2% B27, 0.3 mM L-glutamine, and 100 μ g/ml penicillin/streptomycin). Thereafter, half of the NBA was changed every 3 d. NBA was replaced with B27 reduced minus antioxidant medium (NBA minus AO, 2% B27, and 0.3 mM glutamine) before needle scratch injury.

Microglia cultures were prepared from cerebral cortices of postnatal 0 or 1 (P0 or P1) mice pups with a mild trypsinization method, which exhibited a more quiescent phenotype compared with microglia isolated by shaking, as we described previously (Lin et al., 2017). After removing the meninges, cortical tissues were digested with 0.05% trypsin-EDTA for 15 min at 37°C, followed by centrifugation at 1000 rpm for 1 min. The supernatant was removed, and DMEM/F12 with 10% FBS was added for mechanical trituration. The mixed cortical cells were filtered with a 70 μ m nylon mesh cell strainer (Fisher Scientific, catalog #501960596) and plated on noncoated plastic 6-well plates at proper density (cortical cells from two heads were plated into one plate) in DMEM/F12 with 10% FBS. The media was completely replaced every 2–3 d. After culture for 14 d, mixed cell cultures were mildly trypsinized with a diluted trypsin solution (0.05% trypsin-EDTA diluted 1:1 in DMEM/F12) for 20–30 min to detach an intact layer of cells. The remaining microglia were further cultured in fresh DMEM/F12 with 10% FBS overnight to allow them to recover to resting conditions. Subsequently, the microglia were harvested by trypsinization with 0.05% trypsin-EDTA for 2 min, followed by centrifugation at 1000 rpm for 5 min, and further resuspended in DMEM/F12 complete medium or Neurobasal A medium (without AO, plus 2% B27 and 0.3 mM glutamine); in our experience, the first passage of microglia from each 6-well plate of mixed glia from 2 pups will yield $\sim 3\text{--}5 \times 10^5$ cells.

Needle scratch injury model in cultured neurons

The neuron needle scratch insult was used to mimic the primary mechanical injury of TBI as we and other groups previously described with slight modification (X. Wang et al., 2002; Bae et al., 2018). Briefly, primary mouse cortical neurons were manually scratched using a sterile pipette tip (Corning 0.5–10 μ l, 4901) to produce a linear tear across the culture well. In each well of 6-well and 12-well culture plates, 11×11

scratches and 6×6 scratches were respectively induced, producing a 3 mm grid. Cultures were incubated without a change of the medium. Nonscratched cells were used as control. The cultures were returned to the incubator for indicated time points.

Microglial activation in neuron and microglia coculture

The *in vitro* neuronal and microglia coculture model of TBI was modified based on an *in vitro* model of ischemic penumbra-microglial activation (Kaushal and Schlichter, 2008). There are three stages to this experimental paradigm (see Fig. 1A).

Stage 1. This initial stage was designed to create a needle scratch injury in primary mouse cortical neurons, as neurons are the most vulnerable brain cells for the primary injury after TBI (Frankowski et al., 2022), and injured neurons can rapidly release DAMPs, including ATP and HMGB1 (Wofford et al., 2019), to trigger pro-inflammatory activation (Weber et al., 2015). Primary mouse cortical neurons on days 7–8 were cultured at a humidified (5% CO₂, 37°C) incubator overnight, followed by the needle scratch procedure.

Stage 2. This second stage was designed to assess neuronal needle scratch injury-induced microglial activation. Coculturing of neurons and microglia was performed as described previously (Roque and Costa, 2017). Primary mouse microglia (2×10^5 cells per insert of 12-well inserts or 8×10^5 cells per insert of 6-well inserts) were cultured in the transwell upper permeable insert (3- μ m-diameter pores, Corning, REF3402 or REF3414) with or without 10 mm coverslips (for immunostaining of primary mouse microglia). The original DMEM/F12 media (with 10% FBS) for the primary mouse microglia was gradually replaced with the NBA medium (supplement with 2% B-27 minus AO) with a ratio change over slowly (50:50, 25:75, 0:100) to allow the cells to acclimate to the difference in nutrient content and remain in a relative resting condition. After 48 h, the primary mouse microglia in inserts were then placed onto the culture wells of the needle scratched-primary cortical neurons to be activated for 6 or 24 h. To test the effect of the needle scratch-injured neurons in triggering pro-inflammatory activation of the cocultured microglia, we examined NLRP3 and NF- κ B activation, as well as mRNA levels of pro-inflammatory cytokines *IL-1 β* , *IL-6*, and *TNF α* , while HMGB1 (100 ng/ml) or LPS (100 ng/ml) was added into the top chamber above the naive neurons, and HMGB1 or LPS effects were tested as positive controls of inflammatory activators (Gao et al., 2011). Experimental compounds, such as TAK242 (1 μ M), A804598 (10 μ M), or 3PO (10 μ M), were then added into the upper permeable insert of the primary mouse microglia.

Stage 3. The final stage sought to determine whether the microglia stimulated by scratched neurons developed a neurotoxic phenotype. Activated microglia in the transwell upper permeable inserts were placed on the top of naive neurons for 48 h to induce neurotoxicity.

Cell viability assay

Cell viability of neurons was measured by MTT reduction assays according to the manufacturer's protocol, as we described previously (Liu et al., 2018). Briefly, neurons were treated with fresh DMEM containing MTT for 4 h in a cell culture incubator. The medium was subsequently aspirated, and formazan crystals were dissolved by DMSO. The absorbance at 570 nm was measured by using a microplate reader (SpectraMax M5, Molecular Devices).

LDH release assay

Cell injury was analyzed by measuring LDH release from the medium collected at time points ranging from 1 to 24 h after injury using the LDH-Cytotoxicity Assay Kit (BioVision) according to the manufacturer's instructions. The optical density at 490 nm was measured using a microplate reader (SpectraMax M5, Molecular Devices).

Extracellular ATP measurement

A luciferin/luciferase assay (ENLITEN ATP Assay System Bioluminescence Detection Kit, Promega) was performed to quantitate levels of extracellular ATP in the medium of the neuron culture. Briefly, the medium

was collected at indicated time points after needle scratch injury and centrifuged at 4°C, $1000 \times g$ for 10 min to remove debris, and filtered with 0.22 μ m pore size Millex Filters (Millipore). ATP levels were analyzed immediately after the above procedure; 100 μ l of the media was mixed with 100 μ l of luciferin/luciferase reagent dissolved in dilution buffer, and chemiluminescence values (RLU) were measured with a microplate reader (SpectraMax M5, Molecular Devices).

ELISA

HMGB1 levels in the media of neuronal cultures and serum at indicated time points were detected by mouse ELISA using the HMGB1 RTU ELISA kit (MyBioSource, MBS459874) following the manufacturer's protocol at indicated time points. The samples were centrifuged at 2000 rpm for 15 min at 4°C to remove debris, and the supernatant was collected. Standard curves were generated using purified rHMGB1. The absorbance was measured at 450 nm with a microplate reader (SpectraMax M5, Molecular Devices).

Controlled cortical impact (CCI) models in mice

The CCI model was created as we previously described with a slight modification (Cheng et al., 2021a; Liu et al., 2021). Briefly, male mice (10–12 weeks old, 25–30 g) were anesthetized using 2% isoflurane (Anaquest) in 70% N₂O and 30% O₂ with a Fluotec 3 vaporizer (Colonial Medical) and fixed into a stereotaxic apparatus with a gas anesthesia mask. The scalp was opened to expose the skull, and a 5 mm craniotomy was made on the left cerebral hemisphere between the bregma and the λ using a portable trephine drill (Fine Science Tools). CCI was subsequently established by a pneumatically controlled impactor device (TBI-0310) with a 3 mm flat-tip impounder (4.5 m/s impact velocity, 0.65 mm impact depth, and 500 ms duration). Immediately following injury, the injured region was sutured, and mice were allowed to recover in the cages. The duration of the entire surgical procedure was \sim 8 min. Sham control mice were sutured after craniotomy without cortical impact. At 1 h after TBI, mice were intraperitoneally injected with vehicle or 3PO (50 mg/kg, dissolved in 10% Tween-80, 10% DMSO, and 80% saline) (Cao et al., 2019).

Brain microglia isolation

At 24 h after TBI, microglia from the ipsilateral hemisphere were isolated by Percoll gradient and centrifugation steps as described previously with slight modification, which showed that the purity of microglia isolated was $>90\%$ (de Haas et al., 2007; Wohleb et al., 2011). Briefly, the brain tissue is first homogenized through a 40 μ m strainer with cold PBS on ice, followed by centrifugation at 4°C, $700 \times g$ for 10 min. The pellet was subsequently resuspended with 3.5 ml of ice-cold 75% Percoll, which was then overlaid with 5 ml of ice-cold 25% Percoll; 3 ml ice-cold $1 \times$ PBS was then added to the 25% Percoll layer. The density gradient was then centrifuged at 4°C, $800 \times g$ for 25 min (acceleration = 1, deceleration = 0), whereupon the myelin was removed, and the interphase containing the microglial layer was collected. Isolated cell suspension was washed and then labeled with CD11b immunomagnetic beads and magnetically separated to further purify for microglia (MojoSort Mouse CD11b Selection Kit, catalog #480110). Cells were washed with cold $1 \times$ PBS and centrifuged at 4°C, $700 \times g$ for 10 min; cells suspension was snap-frozen in liquid nitrogen and stored at -80°C before use.

Cytokine proteome profiler array

The inflammatory cytokines in brain microglia or primary microglia were analyzed using the Mouse Cytokine Proteome Profiler Array Panel A kit (R&D Systems) according to the manufacturer's specifications as we described previously (Liu et al., 2021). Briefly, the array membranes were blocked with $1 \times$ blocking buffer, while 80 μ g microglia lysate was incubated for 1 h at room temperature with the supplied cytokine array panel A antibody cocktail. The array membranes were incubated with the lysate-antibody mixtures overnight at 4°C on a platform shaker and washed, and further incubated with streptavidin-HPRP in a blocking buffer for 30 min at room temperature before mixing with the Chemi

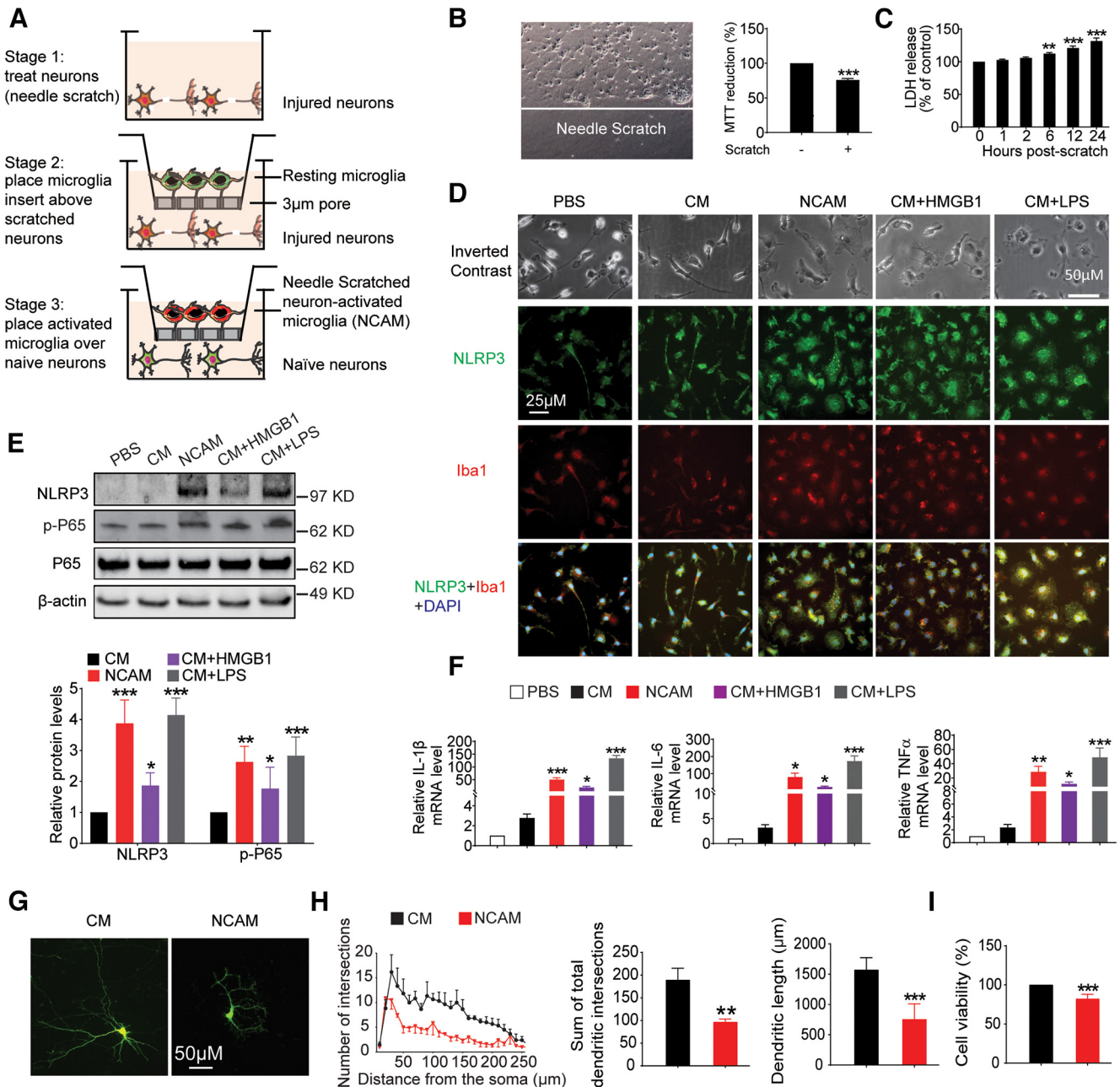


Figure 1. Establishment of the *in vitro* TB1 model of microglial activation. **A**, Schematic representation of neuron-microglia coculture TB1 model. The cortical neurons were needle scratched at Stage 1, and the microglia inserts were placed above the NSNs and cocultured at Stage 2, and the activated microglial cells on inserts were placed on the top of the naive neuron and cocultured at Stage 3. **B**, Representative images of NSNs, MTT reduction of neurons after needle scratch injury. $n = 4$. Student's t test, $t = 13.07$, $p < 0.001$ versus no scratch. Data are mean \pm SEM. *** $p < 0.001$ versus no scratch. **C**, LDH release in the medium of NSN was determined. $n = 4$. One-way ANOVA with Bonferroni *post hoc* test. $F_{(5,18)} = 40.95$, $p < 0.0001$. 1 h versus 0 h: $t = 0.9130$, $p > 0.9999$; 2 h versus 0 h: $t = 2.137$, $p = 0.2328$; 6 h versus 0 h: $t = 4.304$, $p = 0.0021$; 12 h versus 0 h: $t = 7.926$, $p < 0.0001$; 24 h versus 0 h: $t = 11.70$, $p < 0.0001$. Data are mean \pm SEM. ** $p < 0.01$, *** $p < 0.001$ versus 0 h. **D**, Representative inverted contrast and immunofluorescent staining of IBA1 and NLRP3 in primary cultured microglia cocultured with naive neurons (CM), primary cultured microglia cocultured with needle scratched neurons (NCAM), or primary cultured microglia cocultured with naive neurons (CM) and treated with HMGB1 (100 ng/ml) or LPS (100 ng/ml) for 24 h. Scale bar, 25 μ m. **E**, Representative Western blotting analysis of NLRP3, p-P65, and P65 protein levels in NCAM or CM with or without treatment with HMGB1 or LPS. β -actin served as an equal loading control. $n = 4$. One-way ANOVA with Bonferroni *post hoc* test. NLRP3: $F_{(3,12)} = 34.96$, $p < 0.0001$. NCAM versus CM: $t = 7.933$, $p < 0.0001$; CM+HMGB1 versus CM: $t = 2.695$, $p = 0.0478$; CM+LPS versus CM: $t = 8.693$, $p < 0.0001$; p-P65: $F_{(3,12)} = 12.31$, $p = 0.0006$. NCAM versus CM: $t = 4.868$, $p = 0.0012$; CM+HMGB1 versus CM: $t = 2.693$, $p = 0.0486$; CM+LPS versus CM: $t = 5.481$, $p = 0.0004$. Data are mean \pm SEM. * $p < 0.05$, ** $p < 0.01$ versus CM. For the original images of Western blotting analysis of NLRP3, p-P65, P65, and β -actin in Figure 1E, also see Extended Data Figure 1-1. **F**, qRT-PCR analysis of mRNA levels of IL-1 β , IL-6, and TNF α in NCAM or CM with or without treatment with HMGB1 or LPS. One-way ANOVA with Bonferroni *post hoc* test. IL-1 β : $F_{(4,15)} = 147.8$, $p < 0.0001$. CM versus PBS: $t = 0.2658$, $p > 0.9999$; NCAM versus PBS: $t = 7.616$, $p < 0.0001$; CM+HMGB1 versus CM: $t = 2.986$, $p = 0.0369$; CM+LPS versus CM: $t = 20.68$, $p < 0.0001$; IL-6: $F_{(4,15)} = 34.00$, $p = 0.0002$. CM versus PBS: $t = 0.1303$, $p > 0.9999$; NCAM versus PBS: $t = 3.254$, $p = 0.0346$; CM+HMGB1 versus CM: $t = 2.9014$, $p = 0.0433$; CM+LPS versus CM: $t = 7.083$, $p = 0.0001$; TNF α : $F_{(4,15)} = 17.48$, $p < 0.0001$. CM versus PBS: $t = 0.2120$, $p > 0.9999$; NCAM versus PBS: $t = 3.841$, $p = 0.0064$; CM+HMGB1 versus CM: $t = 2.731$, $p = 0.0278$; CM+LPS versus CM: $t = 7.055$, $p < 0.0001$. Data are mean \pm SEM. * $p < 0.05$, ** $p < 0.01$, *** $p < 0.001$ versus PBS. **G**, Representative images of cortical neurons that were transfected with pEGFP-C1 vector for 24 h, followed by coculture with NCAM for another 48 h. Scale bar, 50 μ m. **H**, Total dendritic complexity was analyzed using ImageJ software loaded with the Sholl analysis plug-in, and the simple neurite tracer analysis plug-in. The number of total dendritic intersections and lengths were quantified. $n = 8$ neurons per group. Student's t test, Sum of total dendritic intersections: $t = 3.998$, $p = 0.0013$ versus CM. Dendritic length: $t = 7.179$, $p < 0.0001$ versus CM. Data are mean \pm SEM. ** $p < 0.01$, *** $p < 0.001$ versus CM. **I**, Cell viability was determined by MTT assay. $n = 5$. Student's t test, $t = 6.821$, $p = 0.0001$ versus CM. Data are mean \pm SEM. *** $p < 0.001$ versus CM.

reagent mix. Images were then captured with Bio-Rad ChemiDoc™ MP Imaging System. ImageJ was used to quantify and determine spot density.

qRT-PCR

qRT-PCR was performed as we described previously with slight modification (Liu et al., 2021). Briefly, total RNA from isolated brain microglia and primary mouse microglia was isolated with the miRNeasy micro kit (QIAGEN) according to the manufacturer's instruction and quantified by a DS-11 spectrophotometer (DeNovix). cDNA was prepared from 0.5 μ g of total RNA using QuantiTect Rev Transcription Kit (QIAGEN). qRT-PCR was performed using TaqMan Fast Advanced Master Mix (Applied Biosystems) in a Q53 real-time PCR system (Applied Biosystems). The TaqMan probes used in the study were as follows: Mm00443258_m1 (*TNFA*), Mm00434228_m1 (*IL-1 β*), Mm01210732_m1 (*IL-6*), Mm00441242_m1 (*CCL2*), Mm00445235_m1 (*CXCL10*), Mm00445553_m1 (*CXCL12*), and Mm01545399_m1 (*HPRT*). qRT-PCR was conducted in triplicate, and the relative expression of target genes (fold change) was determined using the $2^{-\Delta\Delta C_t}$ method with normalization to *HPRT*.

Western blotting

Western blotting was performed as we previously described (Liu et al., 2021). After coculture with scratched neurons, microglia in the inserts of the transwell chambers were washed with $1\times$ PBS, and their proteins were prepared with $1\times$ cell lysis buffer (Cell Signaling) supplemented with protease inhibitors (Fisher Scientific). The resulting protein concentrations were quantified with the Pierce BCA Protein Assays (Fisher Scientific); 20 μ g of microglial proteins was then mixed with NuPAGE Sample Reducing Agent (Fisher Scientific) and Protein Sample Loading Buffer (Fisher Scientific) before denaturing in 75°C heating block for 10 min. The denatured proteins were loaded and separated with 4%–12% NuPAGE gel (Fisher Scientific) and transferred onto the PVDF membrane. The membrane was then blocked with 5% (w/v) fat-free milk in TBST (TBS with 0.1% Tween-20) for 60 min at room temperature, followed by incubation overnight at 4°C with the following primary antibodies: NLRP3 mouse antibody (1:1000, AG-20B-0014-C100), p65 antibody (1:1000, Cell Signaling, 8242s), Phospho-p65 antibody (1:1000, Cell Signaling, 3033s), and β -actin antibody (1:3000, Sigma, A5441). The PVDF membrane was further washed with TBST and incubated with IRDye 800CW goat anti-Rabbit (1:10,000, LI-COR Biosciences, #926-32211) or Goat anti-Mouse IgG StarBright Blue 700 (1:10,000, Bio-Rad, #12004159) secondary antibodies for 1 h at room temperature. After washing with TBST, the images were captured with Bio-Rad ChemiDoc™ MP Imaging System.

Immunofluorescent staining

Immunofluorescent staining was performed as we previously described (Liu et al., 2021). The mice were killed and perfused transcardially with 30 ml of ice-cold PBS and 4% PFA. The brains were removed and fixed overnight in 4% PFA and then transferred into 30% sucrose in 0.1 M PBS, pH 7.4, for 2 d. Brain sections were then sliced into 16- μ m-thick coronal sections with a Leica cryostat (Leica, CM1950). Subsequently, brain sections were blocked with 5% BSA in PBS with 0.1% Triton X-100 at room temperature for 1 h. For immunofluorescence staining of cells, primary mouse microglia (2×10^5 cells) were plated in 10 mm coverslips, which were placed into the transwell inserts of 6-well plates at Stage 2 of the microglia-neuron coculture model. Cell cultures processed for immunofluorescent staining were fixed with 4% PFA in PBS for 15 min and permeabilized with blocking buffer (containing 1% FBS, 0.1% Triton X-100 in PBS) for 1 h. Brain sections or cells were incubated at 4°C overnight with IBA1 rabbit antibody (1:250, Wako, 019-19741), NLRP3 goat antibody (1:250, Abcam, ab4207), followed by incubation with secondary antibody conjugated to fluorescein (Goat anti-Rabbit IgG (H + L) Highly Cross-Adsorbed Secondary Antibody, AlexaFluor Plus 594, 1:250, Fisher Scientific, A-11037; Donkey anti-Goat IgG (H + L) Cross-Adsorbed Secondary Antibody, AlexaFluor-488, 1:250, Fisher Scientific, A-11055) for 1 h at room temperature. Sections were washed with PBS and mounted using Vectashield with DAPI (Vector Laboratories, H-1200-10). Fluorescent images were acquired using a Nikon Ts2R FL microscope (Nikon).

Measurement of glycolytic stress by Seahorse XFe24 analyzer

Seahorse glycolytic stress analyses were performed as described previously (Sakamuri et al., 2022). To perform Seahorse extracellular acidification rate (ECAR) analyses of primary mouse microglia or isolated brain microglia, 1×10^5 cells were seeded into each well of the Seahorse XFe24 culture plates and cultured at a 37°C incubator. The cell media was replaced with Seahorse XF Base Medium containing 2 mM L-glutamine and incubated for 45 min at 37°C without CO₂. Seahorse XF Glycolysis Stress Test Kit (catalog #103020-100) was used, and the assay drugs, including glucose (100 mM, 56 μ l), oligomycin (10 μ M, 62 μ l), and 2-DG (500 mM, 69 μ l), were loaded into port A, B, and C of the cartridge. The cartridge was loaded into the Seahorse XFe24 Analyzer for calibration. After calibration, ECAR was measured.

Targeted metabolite analyses and in vitro metabolic tracing

Primary mouse microglia cocultured with needle-scratched neurons (NSNs) were rapidly washed with warm PBS and cultured in either glucose-free DMEM, supplemented with 25 mM of U-¹³C-glucose (Cambridge Isotopes, CLM-1396) for 15 min (Yuan et al., 2019), or glutamine free DMEM, supplemented with 4 mM of U-¹³C-glutamine (Cambridge Isotopes, CLM-1822-H) for 30 min (C. Yang et al., 2014; Yuan et al., 2019). Cells were subsequently washed with ice-cold PBS, and polar metabolites were extracted with methanol-chloroform phase separation (2 ml methanol, 2 ml water, and 4 ml chloroform) as described previously (van Gastel et al., 2020). The sample in the top phase was dried under nitrogen flow, and analyzed by HPLC and High-Resolution Mass Spectrometry and Tandem Mass Spectrometry (LC-MS/MS) at the Harvard Center for Mass Spectrometry; 5 μ l of sample or standard was injected into a ZIC-PHILIC peek-coated column (150 mm \times 2.1 mm, 5 μ m particles, maintained at 40°C, Sigma Aldrich). Buffer A was 20 mM ammonium carbonate, 0.1% ammonium hydroxide in water, and Buffer B was 97% acetonitrile in water. The LC program was as follows: starting at 99% B, to 40% B for 17 min, then to 0% B for 10 min, maintained at 0% B for 5 min, then back to 99% B for 4 min, and re-equilibrated at 99% B for 11 min. For targeted analyses, a standard mix of 1 μ M for each compound of interest was prepared and run after each sample to confirm retention times. Metabolite measurements were normalized to the internal 13C/15N-labeled amino acid standard. Targeted metabolites were analyzed by MetaboAnalyst 5.0 (<http://www.metaboanalyst.ca/>), and metabolite concentration changes were presented as a clustered heatmap (Pang et al., 2021).

Quantification of U-¹³C-metabolites was performed using Tracefinder (version 4.1, Fisher Scientific) (Yuan et al., 2019). The combined extracted ion chromatogram for all m/z corresponding to all isotopologues for each compound was plotted, and the corresponding peak area was integrated. The total combined concentration of all isotopologues for each compound was calculated using the area divided by the area of the IS and using the standard curves. The internal standard used for each compound was the labeled amino acid with strong ionization in the same ion mode and the closest retention time with each compound to quantify.

Plasmid transfection

Primary mouse cortical neurons on glass coverslips in 6-well plate on days 6–7 after seeding were transfected with pEGFP-C1 vector using Lipofectamine 3000 following the manufacturer's protocol as we described previously (Liu et al., 2018). Briefly, a DNA-P3000 mix was prepared by diluting 2.0 μ g of pEGFP-C1 vector in 125 μ l of Opti-MEM I Reduced Serum Media (Fisher Scientific), followed by adding 5 μ l of P3000. Meanwhile, Lipofectamine 3000 mix was prepared by adding 3.75 μ l of Lipofectamine 3000 into 125 μ l of Opti-MEM I Reduced Serum Media. The DNA-P3000 mix was then added to the tube of Lipofectamine 3000 mix and incubated for 10 min at room temperature. Next, the DNA-lipid complex was added to the primary mouse cortical neurons with the NBA (2% B27, minus AO). After culturing for 2 h, the medium was replaced with a fresh NBA, and transfected neurons were cultured for 2 d.

Simple neurite tracer analysis and Sholl analysis

For assessment of neuron morphology and neuronal complexity, pEGFP-C1 vector-transfected neurons were observed and captured by a Nikon Ts2R FL microscope (Nikon). For quantitative analyses, observers were blinded to the experimental groups. Dendritic complexity analysis was performed with ImageJ software loaded with the Sholl analysis plug-in, while the dendritic length was analyzed by ImageJ software loaded with the simple neurite tracer analysis plug-in as described previously (McNair et al., 2010).

Statistical analysis

All data were expressed as mean \pm SEM for at least three independently repeated experiments. Statistical analyses for measurements between two groups were determined by Student's *t* test, and multiple groups were determined by one-way or two-way ANOVA, followed by the Bonferroni *post hoc* test. All statistical analyses were conducted using GraphPad Prism 7 software (GraphPad Software). $p < 0.05$ was considered statistically significant. All statistics are reported in the figure legends.

Results

Establishment of the *in vitro* TBI model of microglial activation

Neuronal needle scratch injury induces microglial activation

In the first set of experiments, we established *in vitro* TBI model of microglial activation following the three stages (Fig. 1A). The first stage established a primary mechanical neuronal injury in primary cultured mouse cortical neurons, the neuronal needle scratch injury model as we previously described (X. Wang et al., 2002). The needle scratch injury directly induced 24.1% neuronal cell death examined with MTT production assay at 2 h after needle scratch (Fig. 1B), followed by 12.3%, 21.1%, and 31.6% progressive neurotoxicity at 6, 12, and 24 h after needle scratch, respectively (Fig. 1C).

The second stage used the needle scratch-injured neuron cultures (NSNs) to trigger a pro-inflammatory activation by coculturing the injured neurons with primary cultured mouse microglia. Immediately after the needle scratch procedure, the naive microglia (cultured with transwell insert) were moved onto the wells of the injured neuronal cultures, and cocultured for 24 h (Fig. 1A). Sister cultures of microglial cells treated with HMGB1 or LPS served as positive controls of inflammatory activation (Fig. 1D; Extended Data Fig. 1-1). Our results showed that after 24 h cocultured, NSN-induced microglia (NCAM) displayed an amoeboid morphology with visible deramification and enlarged cell bodies, which is similar to the morphologic alterations under exposures with HMGB1 or LPS. Microglia cultured with control normal neurons (CM) displayed a typical ramified morphology (Fig. 1D). Moreover, microglia cocultured with injured neurons displayed significant increases in protein levels of inflammasome component NLRP3 and NF κ B activation marker p-p65 (Fig. 1E), as well as increased mRNA levels of pro-inflammatory cytokines *IL-1 β* , *IL-6*, and *TNF α* (Fig. 1F), which were also observed in naive neuron cocultured microglia exposed by HMGB1 and LPS (Fig. 1E,F). These inflammatory activation responses of microglia cocultured with injured neurons were consistent with cultured microglia treated with positive control stimulators, including HMGB1 and LPS, suggesting a pro-inflammatory phenotype.

Activated microglial cells induce neurodegeneration

The third stage used the activated microglia to induce neuronal toxicity. Activated microglia (cultured with transwell insert) were moved into the wells of naive primary neuronal cell cultures. After 48 h, we observed a significantly lower dendritic intersection number (Fig. 1G,H) and decreased neurite lengths for the cocultured naive neurons (Fig. 1G,H). Moreover, the MTT

assay showed that coculture significantly induces neurotoxicity (Fig. 1I), demonstrating the successful establishment of the *in vitro* TBI model of pro-inflammatory activation of microglia, which can trigger neurodegeneration.

Comparable pro-inflammatory gene profiling of the *in vitro* TBI model of microglial activation with the brain microglia of TBI mice

To evaluate the newly established *in vitro* TBI model of microglial activation, we compared the pro-inflammatory profiles between two microglial cell groups, including activated microglia at 24 h after cocultured with the needle scratch-injured neurons *in vitro* (Fig. 2A) and isolating brain microglia at 24 h after TBI in mice (Fig. 2B). Cytokine array (with a capacity of detecting 40 mouse cytokines and chemokines) results showed elevation of 19 pro-inflammatory cytokines and chemokines in the *in vitro* activated microglia, and 22 in brain isolated microglia of TBI mice, compared with their normal controls. Notably, 15 elevated cytokines and chemokines overlapped from the *in vitro* (Fig. 2C) and *in vivo* (Fig. 2D) derived microglia, including *IL-1 α* , *IL-1 β* , *IL-1 α* , *IL-2*, *IL-16*, *IL-23*, *CXCL10*, *CXCL1*, *CCL2*, *CCL3*, *CXCL2*, *CCL5*, *CXCL12*, *TIMP-1*, and *TNF α* , although the relative fold changes of some pro-inflammatory cytokines in the two models are not comparable (Extended Data Fig. 2-1). qRT-PCR further validated these observations in NCAM (Extended Data Fig. 2-2) and TBI microglia (Extended Data Fig. 2-3). Moreover, immunostaining analysis of NLRP3 inflammasome, a biomarker of pro-inflammatory activated microglia after TBI [40], demonstrated that NLRP3 was robustly induced in the *in vitro* microglial activation TBI model (Fig. 1D,E) and in the brain microglia at 24 h after TBI (Extended Data Fig. 2-4). These results demonstrate that the early pro-inflammatory profile of microglia activation in our newly established *in vitro* TBI model is similar to the activated microglia after TBI in mice.

Validation and definition of the role of the neuronal death-derived DAMPs in the *in vitro* TBI model of microglial activation

In the second set of experiments, we applied this *in vitro* TBI model to validate the role of two neuronal death-derived DAMPs, including ATP and HMGB1, in triggering pro-inflammatory activation (Weber et al., 2015). As expected, we observed that needle scratches increased the release of ATP (Fig. 3A) and HMGB1 (Fig. 3B) from the injured neurons. Next, we determined the effect of P2X7R antagonist (A804598) and TLR4 specific inhibitor (TAK242) on ATP and HMGB1-mediated microglial activation by quantitative examinations of NF κ B activation, NLRP3 inflammasome, and pro-inflammatory cytokine production (Fig. 3C). The results showed that TAK242 or A804598 exposure significantly attenuate needle scratch neuronal injury-induced NF κ B (p-P65) levels (Fig. 3D; Extended Data Fig. 1-1), NLRP3 expression (Fig. 3D,E; Extended Data Fig. 1-1), and pro-inflammatory cytokine mRNA expression, including *TNF α* , *IL-6*, and *IL-1 β* (Fig. 3F) in the activated microglia. TAK242 or A804598 exposure has no effect on pro-inflammatory cytokines expression and viability (Extended Data Fig. 3-1) of the naive neuron-cocultured microglia (CM). To exclude the anti-inflammatory effects of TAK242 or A804598 on microglia not through acting on injured neurons in the coculture model system, we also collected the media of needle scratch-injured neurons at 24 h after injury and transferred to naive microglia cultures with or without the addition of A804598 or TAK242, for another 24 h. As expected, the collected medium from injured neurons significantly

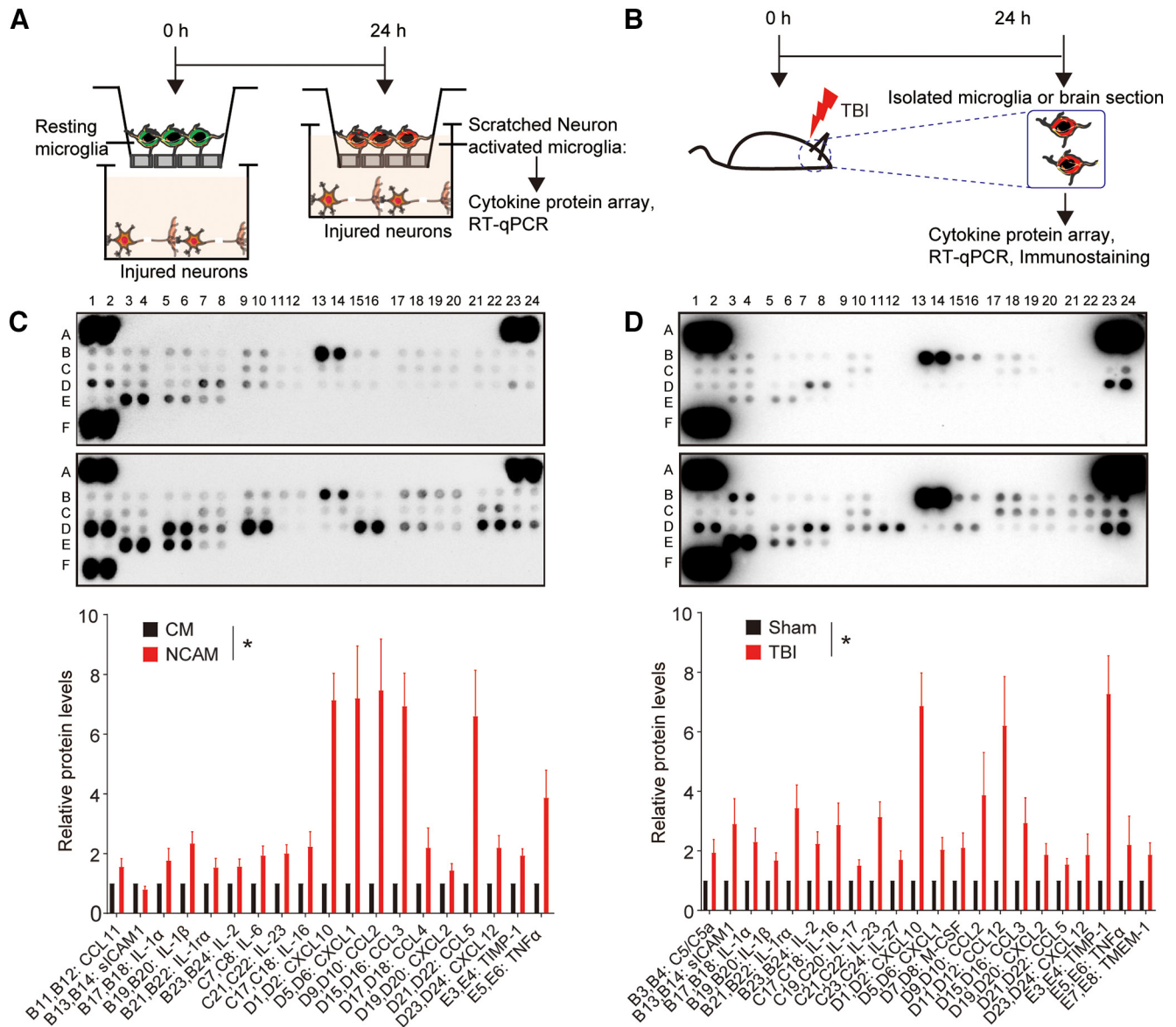


Figure 2. The effect of NSN and TBI on microglia pro-inflammatory profiles. **A**, Scheme for preparing NCAM to analyze pro-inflammatory profile. **B**, Scheme for preparing brain microglia to analyze pro-inflammatory profile. **C**, Representative cytokines profile array and quantitative analysis in NCAM at 24 h after coculture with NSN. $n = 3$. Student's t test. B11, B12: CCL11, $p = 0.025$; B13, B14: sICAM1, $p = 0.033$; B17, B18: IL-1 α , $p = 0.03$; B19, B20: IL-1 β , $p = 0.004$; B21, B22: IL-1 α , $p = 0.039$; B23, B24: IL-2, $p = 0.018$; C7, C8: IL-6, $p = 0.007$; C17, C18: IL-16, $p = 0.013$; C21, C22: IL-23, $p = 0.004$; D1, D2: CXCL10, $p < 0.0001$; D5, D6: CXCL1, $p = 0.004$; D9, D10: CCL2, $p = 0.003$; D15, D16: CCL3, $p < 0.0001$; D17, D18: CCL4, $p = 0.036$; D19, D20: CXCL2, $p = 0.031$; D21, D22: CCL5, $p = 0.003$; D23, D24: CXCL12, $p = 0.007$; E3, E4: TIMP-1, $p = 0.002$; E5, E6: TNF α , $p = 0.006$. Data are mean \pm SEM. $*p < 0.05$. For the analysis of the relative fold change of pro-inflammatory cytokines in NCAM and TBI-activated microglia, see Extended Data Figure 2-1. For validating the effect of NSN coculture on microglial pro-inflammatory cytokine expression, see Extended Data Figure 2-2. **D**, Representative cytokines profile array and quantitative analysis in isolated brain microglia at 24 h after TBI. $n = 3$. Student's t test. B3, B4: C5/C5a, $p = 0.023$; B13, B14: sICAM1, $p = 0.018$; B17, B18: IL-1 α , $p = 0.008$; B19, B20: IL-1 β , $p = 0.011$; B21, B22: IL-1 α , $p = 0.006$; B23, B24: IL-2, $p = 0.006$; C17, C18: IL-16, $p = 0.012$; C21, C22: IL-23, $p = 0.002$; D1, D2: CXCL10, $p < 0.0001$; D5, D6: CXCL1, $p = 0.013$; D9, D10: CCL2, $p = 0.026$; D15, D16: CCL3, $p = 0.017$; D19, D20: CXCL2, $p = 0.017$; D21, D22: CCL5, $p = 0.011$; D23, D24: CXCL12, $p = 0.041$; E3, E4: TIMP-1, $p = 0.001$; E5, E6: TNF α , $p = 0.046$. E7, E8: TMEM-1, $p = 0.02$. Data are mean \pm SEM. $*p < 0.05$. For validating the effect of TBI on microglial pro-inflammatory cytokines expression, see Extended Data Figure 2-3. For determining the effect of TBI on microglial NLRP3 activation, see Extended Data Figure 2-4.

elevated IL-1 β , IL-6, and TNF α mRNA levels of microglial cultures but was significantly attenuated by A804598 or TAK242, respectively, demonstrating the direct actions of A804598 or TAK242 on the microglial cells (Extended Data Fig. 3-2). Together, this *in vitro* TBI model validates the key role of neuronal death-derived DAMPs in mediating microglial activation.

Microglial metabolic profiling in the *in vitro* TBI model of microglial activation

Next, by using this newly established *in vitro* TBI model, we further characterized the metabolic profile of microglia

and elucidated the role of metabolic reprogramming in mediating their pro-inflammatory activation and associated neurodegeneration.

Needle scratch-injured neuron cultures elevate cellular metabolites of glycolysis and TCA cycle metabolism of the cocultured microglia in the *in vitro* TBI model

We first analyzed the metabolic profile of the *in vitro* activated microglia by LC-MS/MS-based quantification of targeted intracellular metabolites. Notably, activated microglial cells, sampled at 6 h after coculture with the injured neurons

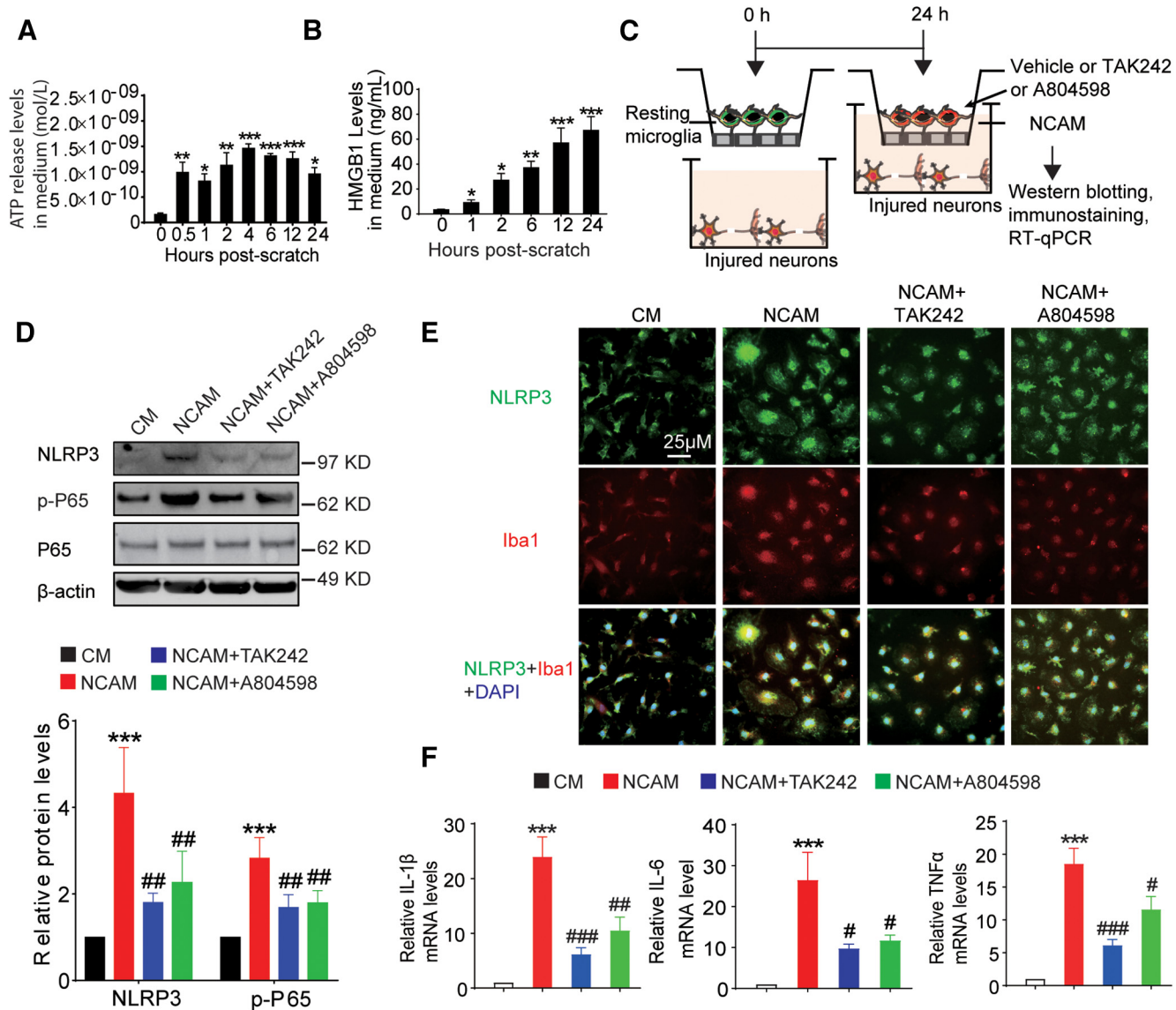


Figure 3. ATP/P2X7R and HMGB1/TLR4 signaling mediated NSN-induced pro-inflammatory microglial activation. **A**, Extracellular ATP (eATP) levels in the medium of NSNs were determined by extracellular ATP assay at the indicated time point. *n* = 3. One-way ANOVA with Bonferroni *post hoc* test. $F_{(7,16)} = 7.057$, $p = 0.0006$. 0.5 h versus 0 h: $t = 3.855$, $p = 0.001$; 1 h versus 0 h: $t = 3.055$, $p = 0.049$; 2 h versus 0 h: $t = 4.513$, $p = 0.0025$; 4 h versus 0 h: $t = 6.075$, $p < 0.0001$; 6 h versus 0 h: $t = 5.375$, $p < 0.0001$; 12 h versus 0 h: $t = 5.12$, $p < 0.0001$; 24 h versus 0 h: $t = 3.713$, $p = 0.0132$. Data are mean ± SEM. **p* < 0.05, ***p* < 0.01, ****p* < 0.001 versus 0 h. **B**, HMGB1 protein levels in the medium of NSN were determined by HMGB1 ELISA at the indicated time point. *n* = 4. One-way ANOVA with Bonferroni *post hoc* test. $F_{(5,18)} = 24.22$, $p < 0.0001$. 1 h versus 0 h: $t = 2.5755$, $p = 0.043$; 2 h versus 0 h: $t = 3.236$, $p = 0.023$; 6 h versus 0 h: $t = 4.660$, $p = 0.001$; 12 h versus 0 h: $t = 7.346$, $p < 0.0001$; 24 h versus 0 h: $t = 8.73$, $p < 0.0001$. Data are mean ± SEM. **p* < 0.05, ***p* < 0.01, ****p* < 0.001 versus 0 h. **C**, Scheme for treating NCAM with TAK242 (1 μM) or A804598 (10 μM) (resting microglia were pretreated with TAK242 or A804598 for 1 h before coculture, and NCAM was further treated with TAK242 or A804598 for 24 h). **D**, Representative Western blotting analysis of NLRP3, p-P65, and P65 protein levels in NCAM with or without treatment with TAK242 or A804598. β-actin served as an equal loading control. *n* = 4. One-way ANOVA with Bonferroni *post hoc* test. NLRP3: $F_{(3,12)} = 19.02$, $p < 0.0001$. NCAM versus CM: $t = 7.231$, $p < 0.0001$; NCAM + TAK242 versus NCAM: $t = 5.491$, $p = 0.001$; NCAM + A804598 versus NCAM: $t = 4.485$, $p = 0.0045$. Data are mean ± SEM. p-P65: $F_{(3,12)} = 22.96$, $p < 0.0001$. NCAM versus CM: $t = 8.213$, $p < 0.0001$; NCAM + TAK242 versus NCAM: $t = 5.119$, $p = 0.0015$; NCAM + A804598 versus NCAM: $t = 4.685$, $p = 0.0033$. Data are mean ± SEM. ****p* < 0.001 compared with CM. ***p* < 0.01 compared with NCAM. #*p* < 0.05, ##*p* < 0.01, ###*p* < 0.001 compared with NCAM. **E**, Representative immunofluorescent staining of NLRP3 and IBA1 in NCAM with or without treatment with TAK242 or A804598. Scale bar, 25 μm. **F**, qRT-PCR analysis of mRNA levels of IL-1β, IL-6, and TNFα in NCAM with or without treatment with TAK242 or A804598. *n* = 4. One-way ANOVA with Bonferroni *post hoc* test. IL-1β: $F_{(3,12)} = 20.10$, $p < 0.0001$. NCAM versus CM: $t = 7.391$, $p < 0.0001$; NCAM + TAK242 versus NCAM: $t = 5.760$, $p < 0.0001$; NCAM + A804598 versus NCAM: $t = 4.377$, $p = 0.0054$; IL-6: $F_{(3,12)} = 10.31$, $p = 0.0012$. NCAM versus CM: $t = 5.465$, $p = 0.0009$; NCAM + TAK242 versus NCAM: $t = 3.608$, $p = 0.0215$; NCAM + A804598 versus NCAM: $t = 3.189$, $p = 0.0467$; TNFα: $F_{(3,12)} = 31.53$, $p < 0.0001$. NCAM versus CM: $t = 9.270$, $p < 0.0001$; NCAM + TAK242 versus NCAM: $t = 6.942$, $p < 0.0001$; NCAM + A804598 versus NCAM: $t = 4.381$, $p = 0.0254$. Data are mean ± SEM. ****p* < 0.001 compared with CM. **p* < 0.05, ***p* < 0.01, ****p* < 0.001 compared with NCAM. For determining the effect of TAK242 and A804598 on naive-neuron cocultured microglial pro-inflammatory cytokines and viability, see Extended Data Figure 3-1. For determining the effect of NSN conditional medium on P2X7R and TLR4 signaling-mediated pro-inflammatory cytokines expression in microglia, see Extended Data Figure 3-2.

(Fig. 4A), exhibited a significant increase of glycolytic intermediates, including lactate, pyruvate, 3-phosphoglycerate, and phosphoenolpyruvate (Fig. 4B). Additionally, there was a dramatic increase in intracellular TCA cycle metabolites,

particularly more pronounced for citrate and aconitate (Fig. 4B). These results indicated that the microglia cocultured with NSNs triggered increases in both cellular glycolysis and mitochondrial TCA cycle activity.

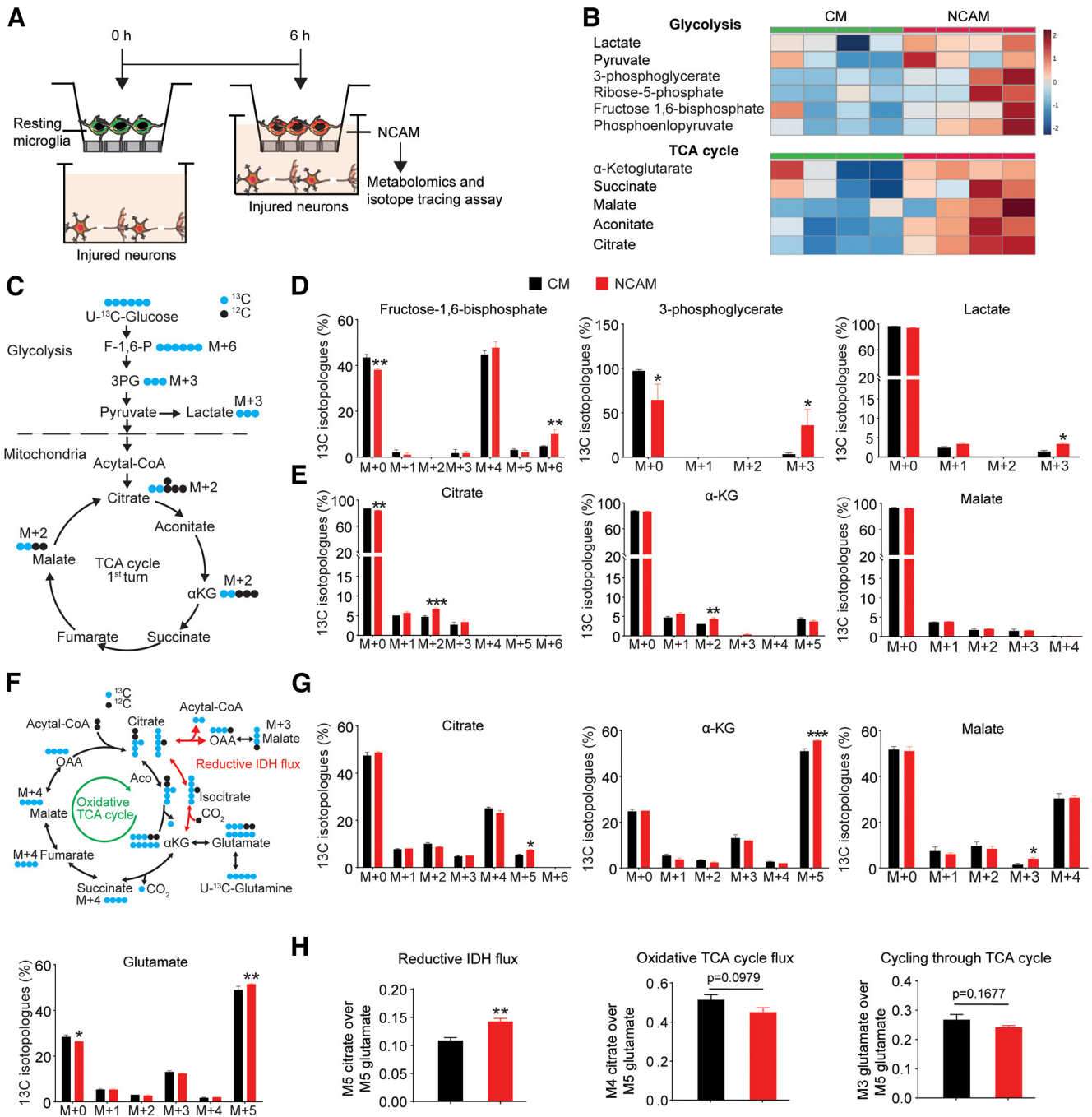


Figure 4. NCAM display increased glycolytic and glutamine reductive metabolism. **A**, Scheme for preparing NCAM to analyze metabolic profiles and flux. **B**, Heatmaps for metabolites of glycolysis and TCA cycles in NCAM at 6 h after coculture with NSN. $n = 4$. Metabolite abundance values were color scaled. **C**, Schematic presentation of the contribution of $U\text{-}^{13}\text{C}$ -glucose-derived carbons to glycolytic and TCA cycle intermediates and amino acids. Blue represents ^{13}C carbons. Black represents ^{12}C carbons. After coculture with NSNs for 6 h, NCAM were cultured in $U\text{-}^{13}\text{C}$ -glucose tracer medium for 15 min. **D**, **E**, Mass isotopomer distributions of glycolytic intermediates, including fructose-1,6-bisphosphate (F-1,6-P), 3-phosphoglycerate (3PG), lactate, and TCA cycle intermediates, including citrate, α -KG, and malate. Two-way ANOVA with Bonferroni *post hoc* test. Fructose-1,6-bisphosphate: $F_{(6,42)} = 6.189$, $p = 0.0001$. NCAM versus CM: $t = 3.939$, $p = 0.0021$ (M + 0); $t = 0.9378$, $p > 0.9999$ (M + 1); $t = 0.000$, $p > 0.9999$ (M + 2); $t = 0.3751$, $p > 0.9999$ (M + 3); $t = 2.063$, $p = 0.3173$ (M + 4); $t = 0.9378$, $p > 0.9999$ (M + 5); $t = 3.939$, $p = 0.0021$ (M + 6); 3-phosphoglycerate: $F_{(3,24)} = 8.481$, $p = 0.0005$. NCAM versus CM: $t = 3.138$, $p = 0.0207$ (M + 0); $t = 6.355e-016$, $p > 0.9999$ (M + 1); $t = 3.178e-016$, $p > 0.9999$ (M + 2); $t = 2.922$, $p = 0.0337$ (M + 3); lactate: $F_{(3,24)} = 5.742$, $p = 0.0041$. NCAM versus CM: $t = 2.125$, $p = 0.0656$ (M + 0); $t = 1.253$, $p = 0.8886$ (M + 1); $t = 0.000$, $p > 0.9999$ (M + 2); $t = 2.716$, $p = 0.0483$ (M + 3); citrate: $F_{(6,42)} = 5.830$, $p = 0.0002$. NCAM versus CM: $t = 4.006$, $p = 0.0017$ (M + 0); $t = 1.001$, $p > 0.9999$ (M + 1); $t = 4.256$, $p = 0.0008$ (M + 2); $t = 0.5007$, $p > 0.9999$ (M + 3); $t = 0.000$, $p > 0.9999$ (M + 4); $t = 0.000$, $p > 0.9999$ (M + 5); $t = 0.000$, $p > 0.9999$ (M + 6); α -KG: $F_{(5,36)} = 4.375$, $p = 0.0033$. NCAM versus CM: $t = 1.716$, $p = 0.5683$ (M + 0); $t = 2.288$, $p = 0.1686$ (M + 1); $t = 3.432$, $p = 0.0091$ (M + 2); $t = 0.5721$, $p > 0.9999$ (M + 3); $t = 0.000$, $p > 0.9999$ (M + 4); $t = 1.716$, $p = 0.5683$ (M + 5); malate: $F_{(4,30)} = 1.824$, $p = 0.1503$. NCAM versus CM: $t = 2.316$, $p = 0.1380$ (M + 0); $t = 0.6814$, $p > 0.9999$ (M + 1); $t = 0.8164$, $p > 0.9999$ (M + 2); $t = 0.8936$, $p > 0.9999$ (M + 3); $t = 0.09504$, $p > 0.9999$ (M + 4). Data are mean \pm SEM. * $p < 0.05$, ** $p < 0.01$ versus CM. **F**, Schematic presentation of the contribution of $U\text{-}^{13}\text{C}$ -glutamine-derived carbons to TCA cycle intermediates and amino acids. Blue represents ^{13}C carbons. Black represents ^{12}C carbons. After coculture with NSNs for 6 h, NCAM were cultured in $U\text{-}^{13}\text{C}$ -glutamine tracer medium for 30 min. Two-way ANOVA with Bonferroni *post hoc* test. Citrate: $F_{(6,42)} = 3.946$, $p = 0.0032$. NCAM versus CM: $t = 1.614$, $p = 0.7983$ (M + 0); $t = 0.8069$, $p > 0.9999$ (M + 1); $t = 2.017$, $p = 0.3505$ (M + 2); $t = 0.8069$, $p > 0.9999$ (M + 3); $t = 2.421$, $p = 0.1392$ (M + 4); $t = 3.228$, $p = 0.0170$ (M + 5); $t = 0.000$, $p > 0.9999$ (M + 6); α -KG: $F_{(5,36)} = 9.797$, $p < 0.0001$. NCAM versus CM: $t = 0.5214$,

Needle scratch-injured neuron cultures increase glucose-derived glycolysis and TCA cycle fragmentation of the cocultured microglia in the *in vitro* TBI model

We further analyzed the metabolic flux of glucose through the TCA cycle using a U-¹³C-glucose tracer (Fig. 4C). Our experimental results showed significant increases in the U-¹³C-glucose-derived fructose-1,6-bisphosphate M + 6 isotopologue, 3-phosphoglycerate M + 3 isotopologue, and lactate M + 3 isotopologue (Fig. 4D), demonstrating an increased glycolytic flux in the NCAM. Moreover, we also analyzed glucose-derived oxidative TCA cycle flux in the activated microglia by determining isotopologues of citrate, α -KG, and malate. We found an increase of U-¹³C-glucose-derived M + 2 isotopologues of citrate and α -KG, but no significant effect on the malate M + 2 isotopologue was detected (Fig. 4E), indicating an increase of glucose-derived oxidative TCA cycle flux, but there was a truncated TCA cycle that might occur at the downstream of α -KG of the activated microglia.

Needle scratch-injured neuron cultures promote glutaminolysis and glutamine reductive metabolism of the cocultured microglia in the *in vitro* TBI model

We also analyzed the metabolic flux of glutamine with U-¹³C-glutamine tracer in microglia at 6 h after cocultured with the injured neuron cultures (Fig. 4F). We observed that the production of the U-¹³C-glutamine-derived M + 5 isotopologues of α -KG was significantly increased, suggesting elevated glutaminolysis in NCAM. Moreover, M + 4 isotopologues of citrate and malate, and M + 3 isotopologue of α -KG and glutamate were not significantly changed, suggesting that NSN coculture has no significant effect on glutamine-derived oxidative metabolism of the TCA cycle in microglia (Fig. 4G). However, there were significant increases of U-¹³C-glutamine-derived M + 5 isotopologues of citrate, and M + 3 isotopologues of malate, suggesting an increase in glutamine-dependent reductive carboxylation of α -KG (reductive IDH flux) in NCAM (Fig. 4G). Last, analysis of relative fluxes determined an increase in reductive IDH flux, while the oxidative TCA cycle flux and cycling through the TCA cycle were not altered (Fig. 4H). These results suggested a significant increase in glutamine reductive metabolism in the NCAM.

Microglial glycolysis elevation leads to the pro-inflammatory activation of microglia and the activation-associated neurodegeneration in the *in vitro* TBI model

Cellular glycolysis elevation leads to the pro-inflammatory activation of microglia in the *in vitro* and *in vivo* TBI model

Our earlier experiments identified metabolic shifts in the acute phase of activated microglia, such as the elevation of glycolysis.

To determine the functional consequences of this shift, we applied pharmacological approaches to test whether blocking glycolysis elevation can inhibit microglial pro-inflammatory activation and alter their functional phenotype in our newly established model.

Activated microglia cells were treated with or without a selective glycolysis inhibitor 3PO (10 μ M) for 6 h (Fig. 5A), Seahorse glycolytic stress assays showed that NSN conditional medium significantly triggered glycolysis elevation in microglia; however, 3PO attenuated the increased glycolysis activity (Fig. 5B). Subsequently, microglia cells were cocultured with NSN and treated with 3PO (10 μ M) for 24 h (Fig. 5C) significantly inhibited their pro-inflammatory activation, reflected by reduced NF κ B activation (Fig. 5D; Extended Data Fig. 1-1) and NLRP3 inflammasome activation (Fig. 5D,E; Extended Data Fig. 1-1). The microglial pro-inflammatory activation inhibition of 3PO was further validated by the detected decreases of mRNA expression of pro-inflammatory cytokines IL-1 β , IL-6, and TNF α (Fig. 5F). 3PO treatment can attenuate pro-inflammatory cytokines expression IL-1 β and TNF α but does not affect the viability (Extended Data Fig. 3-1) of the naive neuron-cocultured microglia (CM), supporting the key role of glycolysis in controlling pro-inflammatory cytokine production in microglia.

Interestingly, we also observed that inhibition of TLR4 by TAK242 attenuated glycolysis activity in the conditional medium-transfer experiment (Extended Data Fig. 5-1). These results demonstrate that the metabolic shift toward increased glycolysis leads to the pro-inflammatory activation of NCAM. To further validate the role of glycolysis in controlling pro-inflammatory activation of brain microglia, 3PO or vehicle was administrated into the CCI model, and glycolysis of brain microglia collected at 4 h after TBI was examined. We observed significantly increased glycolysis and glycolysis capacity in isolated brain microglia, but 3PO can significantly attenuate TBI-induced glycolysis in isolated brain microglia (Extended Data Fig. 5-2). Consistently, 3PO administration significantly reduced the mRNA levels of pro-inflammatory cytokines, including IL-6, IL-1 β , and TNF α (Extended Data Fig. 5-3). Together, these data suggested that cellular glycolysis elevation leads to the pro-inflammatory activation of microglia in the *in vitro* and *in vivo* TBI model.

Cellular glycolysis elevation leads to the microglial pro-inflammatory activation-associated neurodegeneration in the *in vitro* TBI model

It has been proposed that the early pro-inflammatory activation of microglia after TBI causes neurodegeneration (Donat et al., 2017), but whether the metabolic shift-derived microglial pro-inflammatory activation contributes to the direct neurotoxicity of the nearby neurons has not been defined. In this experiment, at Stage 3 of the *in vitro* model, NCAMs with or without 3PO exposures were transferred into cultures of pEGF-C1 transfected naive neurons for 48 h (Fig. 5G). The pEGF-C1 transfected neurons (Fig. 5H) were captured by fluorescent microscope and analyzed by ImageJ software loaded with Sholl analysis and simple neurite tracer analysis (Fig. 5I). The results showed that NCAM treated with 3PO significantly increased dendritic intersections and length (Fig. 5J) and significantly reduced NCAM-mediated neurotoxicity of primary cultured neurons compared with NSN-activated microglia alone (Fig. 5K). Collectively, these results suggest that the microglial metabolic shift toward cellular glycolysis elevation is a key pathogenic mechanism in controlling

←

$p > 0.9999$ (M + 0); $t = 2.085$, $p = 0.2651$ (M + 1); $t = 1.216$, $p > 0.9999$ (M + 2); $t = 1.912$, $p = 0.3834$ (M + 3); $t = 0.5214$, $p > 0.9999$ (M + 4); $t = 6.256$, $p < 0.0001$ (M + 5); malate: $F_{(4,30)} = 2.679$, $p = 0.0507$. NCAM versus CM: $t = 0.5244$, $p > 0.9999$ (M + 0); $t = 1.049$, $p > 0.9999$ (M + 1); $t = 1.223$, $p > 0.9999$ (M + 2); $t = 2.797$, $p = 0.0446$ (M + 3); $t = 0.1748$, $p > 0.9999$ (M + 4); glutamate: $F_{(5,36)} = 5.669$, $p = 0.0006$. NCAM versus CM: $t = 3.036$, $p = 0.0266$ (M + 0); $t = 0.3795$, $p > 0.9999$ (M + 1); $t = 0.3795$, $p > 0.9999$ (M + 2); $t = 1.138$, $p > 0.9999$ (M + 3); $t = 0.3795$, $p > 0.9999$ (M + 4); $t = 4.174$, $p = 0.0011$ (M + 5). Data are mean \pm SEM. * $p < 0.05$, ** $p < 0.01$, *** $p < 0.001$ versus CM. **H**, Determination of relative reductive IDH flux based on U-¹³C-glutamine labeling: ratio of M5 citrate/M5 glutamate; determination of oxidative TCA cycle activity based on U-¹³C-glutamine labeling: ratio of M4 citrate/M5 glutamate; determination of cycling of glutamate through the oxidative TCA cycle based on U-¹³C-glutamine labeling: M3 glutamate/M5 glutamate. $n = 4$. Student's t test. Reductive IDH flux: $t = 3.998$, $p = 0.0071$ versus CM; oxidative TCA cycle flux: $t = 1.959$, $p = 0.0979$ versus CM; cycling through TCA cycle: $t = 1.569$, $p = 0.1677$ versus CM. Data are mean \pm SEM. ** $p < 0.05$ versus CM.

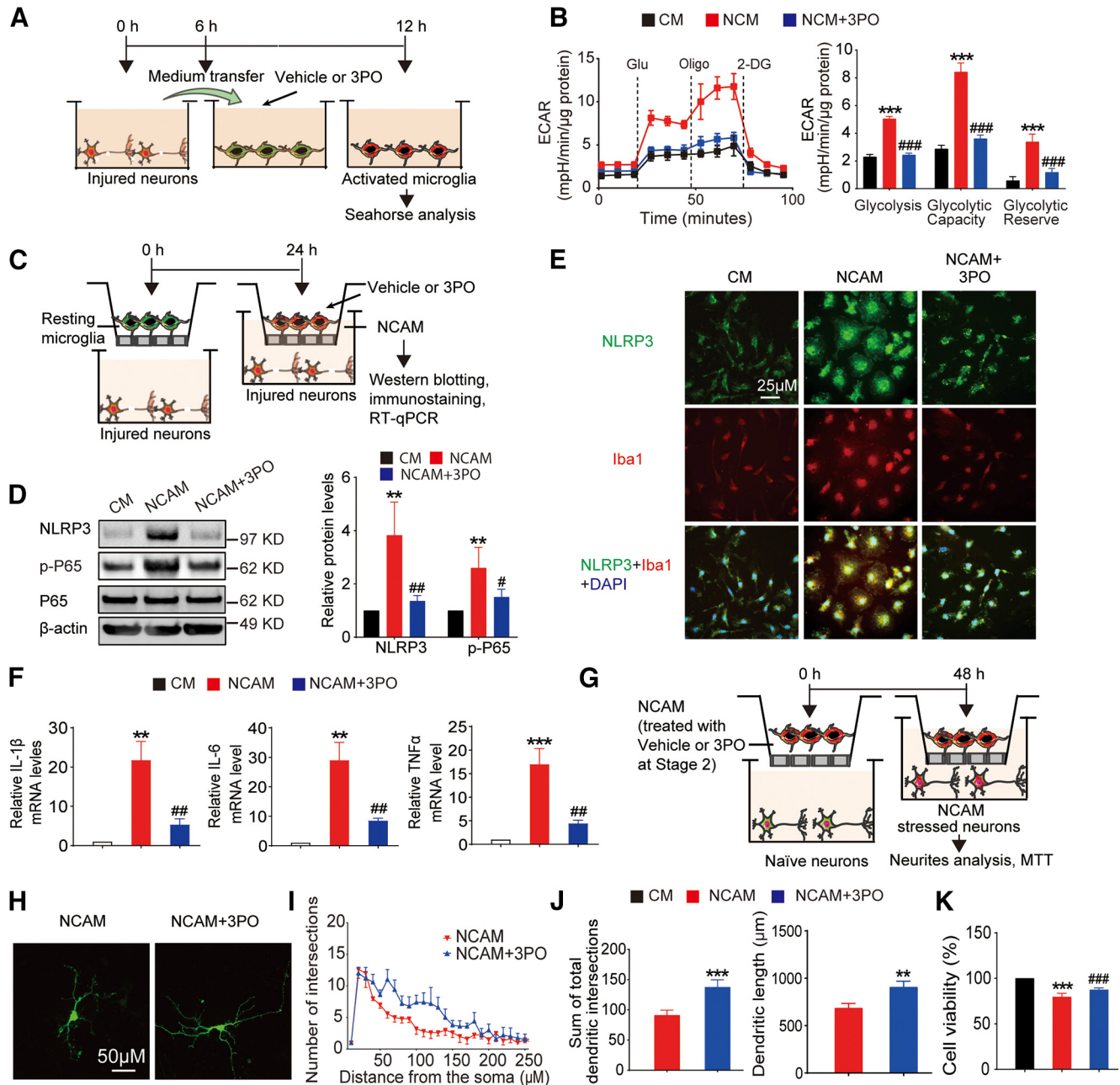


Figure 5. Glycolysis promotes activation of NCAM and inhibition of glycolysis in NCAM attenuates NCAM-induced neuronal injury. **A**, Scheme for cell treatment to analyze glycolysis of NSN conditioning medium-activated microglia. **B**, ECAR of NCAM treated with 3PO (10 μ M) for 6 h after sequential addition of glucose (Glu), oligomycin (Oligo), and 2-DG. $n = 4$. Two-way ANOVA with Bonferroni *post hoc* test. $F_{(4,27)} = 6.305$, $p = 0.001$. Glycolysis: NCAM versus CM: $t = 5.557$, $p < 0.001$; NCAM + 3PO versus NCAM: $t = 5.274$, $p < 0.001$; glycolytic capacity: NCAM versus CM: $t = 11.21$, $p < 0.001$; NCAM + 3PO versus NCAM: $t = 9.715$, $p < 0.001$; glycolytic reserve: NCAM versus CM: $t = 5.653$, $p < 0.001$; NCAM + 3PO versus NCAM: $t = 4.442$, $p < 0.001$. Data are mean \pm SEM. *** $p < 0.001$ versus CM. ### $p < 0.001$ compared with NCAM. For determining the effect of P2X7R and TLR4 signaling on glycolysis in microglia treated with NSN conditional medium, see Extended Data Figure 5-1. For determining the effect of 3PO on glycolysis in microglia after TB1, see Extended Data Figure 5-2. **C**, Scheme for cell treatment to measure the pro-inflammatory profile of NCAM. **D**, Representative gel images of Western blotting analysis of NLRP3, p65, and p-P65 in NCAM, which were treated with 3PO (10 μ M) for 24 h. β -Actin served as an equal loading control. $n = 4$. One-way ANOVA with Bonferroni *post hoc* test. NLRP3: $F_{(2,9)} = 17.89$, $p = 0.0007$. NCAM versus CM: $t = 5.499$, $p = 0.0011$; NCAM + 3PO versus NCAM: $t = 4.789$, $p = 0.0030$; p-p65: $F_{(2,9)} = 11.71$, $p = 0.0031$. NCAM versus CM: $t = 4.739$, $p = 0.0032$; NCAM + 3PO versus NCAM: $t = 3.221$, $p = 0.0314$. Data are mean \pm SEM. ** $p < 0.01$ versus CM. # $p < 0.05$, ## $p < 0.01$ versus NCAM. For the original images of Western blotting analysis of NLRP3, p-P65, P65, and β -actin in Figure 5D, see also Extended Data Figure 1-1. **E**, Representative coimmunostaining of IBA1 and NLRP3 in NCAM, which were treated with 3PO (10 μ M) for 24 h. Scale bar, 25 μ m. **F**, qRT-PCR analysis of mRNA levels of IL-1 β , IL-6, and TNF α in NCAM, which were treated with 3PO (10 μ M) for 24 h. $n = 4$. One-way ANOVA with Bonferroni *post hoc* test. IL-1 β : $F_{(2,9)} = 14.31$, $p = 0.0016$. NCAM versus CM: $t = 5.069$, $p = 0.0020$; NCAM + 3PO versus NCAM: $t = 4.013$, $p = 0.0092$; IL-6: $F_{(2,9)} = 16.58$, $p < 0.001$. NCAM versus CM: $t = 5.561$, $p = 0.001$; NCAM + 3PO versus NCAM: $t = 4.072$, $p = 0.008$; TNF α : $F_{(2,9)} = 18.21$, $p < 0.001$. NCAM versus CM: $t = 5.731$, $p < 0.001$; NCAM + 3PO versus NCAM: $t = 4.502$, $p = 0.004$. Data are mean \pm SEM. ** $p < 0.01$, *** $p < 0.001$ versus CM. ## $p < 0.05$ versus NCAM. For determining the effect of 3PO on naive-neuron cocultured microglial pro-inflammatory cytokines and viability, see Extended Data Figure 3-1. For determining the effect of 3PO on pro-inflammatory cytokine expression in microglia after TB1, see Extended Data Figure 5-3. **G**, Scheme for neurite analysis and MTT analysis of neurons after coculturing with NCAM with or without treatment of 3PO (10 μ M). **H**, Naive cortical neurons were transfected with pEGFP-C1 vector for 24 h, followed by coculture with NCAM on inserts for 48 h. Images are representative photographs of GFP-transfected neurons. Scale bar, 50 μ m. **I**, Total dendritic complexity was analyzed using ImageJ software loaded with the Sholl analysis plug-in and the simple neurite tracer analysis plug-in. **J**, The number of total dendritic intersections and lengths were quantified. $n = 8$ neurons per group. Student's *t* test. Sum of total dendritic intersections: $t = 4.611$, $p = 0.0004$ versus NCAM; dendritic length: $t = 3.226$, $p = 0.0061$ versus NCAM. Data are mean \pm SEM. ** $p < 0.01$ compared with NCAM. **K**, Cell viability was determined by MTT

the inflammatory phenotype of microglia, which also functions in mediating neurotoxicity in the *in vitro* TBI model of microglial activation.

Discussion

In this study, we successfully established a novel *in vitro* model of microglial activation in TBI. By applying this *in vitro* model, we validated that its pro-inflammatory gene expression profile is similar to the *in vivo* post-TBI microglial pro-inflammatory activation. We also characterized metabolic profiles of the pro-inflammatory activated microglia, and defined the role of elevated glycolysis in mediating microglial pro-inflammatory activation and associated neurodegeneration. We believe this newly established *in vitro* model provides a novel and highly translational platform for investigations of primary neuronal injury-induced acute microglial activation and the activation-associated neurodegeneration after TBI.

Although stretch, blast, compression, scratch, shear and fluid percussion injury are the most commonly used mechanical force on the cultured neurons or vascular endothelial cells as in *in vitro* models of TBI (Wu et al., 2021) and oxygen/glucose deprivation were also used as an *in vitro* TBI model of vascular endothelial cell injury (Salvador et al., 2015), an *in vitro* TBI model to closely mimic microglial pro-inflammatory activation and associated neurodegeneration is still lacking. Therefore, the present study aimed to establish a new *in vitro* TBI model of microglial activation. Our model is different from other existing TBI *in vitro* models in (1) we used primary neuron and microglial cocultures; (2) we used needle scratch injury to mimic primary mechanical brain injury; (3) the injured neuronal cultures serve as post-TBI environmental conditions to trigger cocultured microglial activation; and (4) microglial function in mediating neurodegeneration can be also tested in the new model. Through pro-inflammatory cytokines array, we detected increases of some pro-inflammatory cytokines of both the microglia in *in vitro* and *in vivo* TBI model, suggesting that the *in vitro* microglial activation model has certain transparency for the *in vivo* microglial activation after TBI. However, there are some different cytokine expression patterns between the two models, indicating the fact that the *in vitro* model cannot completely replicate the *in vivo* microglial activation responses after TBI. Indeed, it is impossible to make a simple *in vitro* or *in vivo* model to truly mimic the complex pathophysiology of TBI. It is worth noting that heterogeneity is the key feature of human TBI (Covington and Duff, 2021); the currently available animal TBI models can only partially recapitulate some aspects of human TBI pathophysiology (Namjoshi et al., 2014). Furthermore, microglial activation after TBI is complex and dynamic (G. Wang et al., 2013; Gottlieb et al., 2022). In our *in vitro* TBI model of neuron-microglia coculture system, the neurons were first subjected to needle-scratched injury, which may mostly mimic contusion with moderate/severe TBI (Morrison et al., 2011; Kumaria, 2017). One advantage afforded by this new *in vitro* model is that different primary injury models could be incorporated to investigate corresponding injury-associated TBI pathophysiology. For example, needle scratch injury of neurons could be replaced by shear injury, stretch injury, or

compression injury, etc. Moreover, the injury severity of neuron cultures can also be well controlled.

Next, we evaluated this newly established *in vitro* model by determining the effect of neuronal-released ATP and HMGB1, which are two of the most studied DAMPs and were initially released by the injured neurons (Wofford et al., 2019). Moreover, it has been proposed that ATP or HMGB1 can directly cause microglial activation via the receptors P2X7R (Davalos et al., 2005) or TLR4 (Simon et al., 2018), respectively, after TBI. However, this remains to be further elucidated. By using the new *in vitro* model, we found that the released extracellular ATP and HMGB1 from NSN can trigger the pro-inflammatory activation of microglia, and P2X7R antagonist (A804598) or TLR4 specific inhibitor (TAK242) exerts inhibitory roles in NSN-induced microglial pro-inflammatory activation. These results demonstrate that ATP/P2X7R and HMGB1/TLR4 signaling axes play key roles in the *in vitro* TBI model of microglial activation and provide experimental evidence that the primary neuronal injury-released ATP and HMGB1 trigger the early pro-inflammatory activation of brain microglia after TBI. Therefore, this newly established *in vitro* TBI model enables us to better define and elucidate the specific roles and signaling mechanisms in conjunction with specific genetic and pharmacological approaches.

Microglial metabolic reprogramming has been proposed as the convergence point of pathways and mechanisms underlying the pro-inflammatory activation of microglia (Bernier et al., 2020a; S. Yang et al., 2021). However, the alterations of microglia cellular metabolism and its consequences after neurologic disorders, including TBI, remain poorly known (Shi et al., 2020). The major reason is the lack of analytical approaches for the cellular metabolic profile of the single-cell population in the brain. In this *in vitro* TBI model, for the first time, we applied comprehensive metabolic analysis approaches, including LC-MS/MS-based metabolomics, isotope tracing, and Seahorse analyzer. We found that injured neuron cultures lead to a metabolic shift of microglia toward increases in glycolysis, glutaminolysis, and glutamine reductive metabolism, which is consistent with the *in vivo* observation that activated microglia increased utilization of glucose and glutamine (Bernier et al., 2020b). Moreover, we demonstrated that the pro-inflammatory-activated NCAM exhibit an increased truncated TCA cycle that might occur downstream of α -KG in this *in vitro* model. Earlier studies reported that the truncated TCA cycle is an important characteristic of activated dendritic cells (DCs) and macrophages (Martinez-Reyes and Chandel, 2020). In the truncated TCA cycle, glycolysis or glutaminolysis-derived citrate can exit the mitochondria to cytosol, where citrate can be cleaved to oxaloacetate and acetyl-CoA. The cytosolic acetyl-CoA can further contribute to fatty acid synthesis and protein acetylation, both of which contribute to immune cell activation (Williams and O'Neill, 2018). Therefore, our new findings suggest that the truncated TCA cycle, accompanied by increased glycolysis and glutaminolysis, may lead to citrate accumulation and activation of NCAM. However, the roles and molecular mechanisms of glycolysis, glutaminolysis, and truncated TCA cycle on modulating microglial activation and function need to be elucidated in both this *in vitro* TBI model and *in vivo* TBI in the future.

Although it has been suggested that glycolysis is increased in microglia after TBI (Shi et al., 2020), and inhibition of glycolysis can ameliorate microglial activation-related neuroinflammatory

←

assay. $n = 5$. One-way ANOVA with Bonferroni *post hoc* test. $F_{(2,12)} = 100.8$, $p < 0.001$. NCAM versus CM: $t = 14.01$, $p < 0.001$; NCAM + 3PO versus NCAM: $t = 5.010$, $p < 0.001$. Data are mean \pm SEM. *** $p < 0.001$ versus CM. ### $p < 0.001$ versus NCAM.

diseases (Cheng et al., 2021b), whether inhibition of glycolysis can attenuate microglia pro-inflammatory activation and mediated neurodegeneration in TBI remains unclear. By using this new *in vitro* model, we tested the effects of glycolysis inhibitor 3PO, further validated and defined the crucial role of glycolysis elevation in promoting microglial pro-inflammatory activation and mediated neurodegeneration. Interestingly, we found that TLR4 inhibitor TAK242 treatment also significantly attenuates NSN-induced glycolysis in microglia, which is consistent with previous observations (Lauterbach et al., 2019) that TLR4 is a key receptor in eliciting aerobic glycolysis, indicating that glycolysis could be a central hub for connecting pro-inflammatory receptors to downstream signaling pathways. Importantly, our experimental findings also suggest that inhibiting the glycolytic increase of TBI-activated microglia may be a potential therapeutic avenue to restrict activation-mediated neurodegeneration after TBI; this notion is supported by a recent study reporting that glycolytic inhibitor 2-DG significantly inhibited neuronal injury induced by microglial conditioned media (Cheng et al., 2021b). Therefore, we believe that this *in vitro* TBI model of microglial activation is an advantageous tool for testing cellular metabolic disturbance-induced microglial activation and mediated neurodegeneration.

We are aware that there are several caveats. First, this *in vitro* model involves neuron-microglia cocultures, but they are not physically contacted between neurons and microglia, which may limit testing the role of microglial phagocytosis on injured neurons after TBI. Second, this new *in vitro* model may not be applicable to mimic all different types of TBI. The complexity of injuries and associated underlying mechanisms of TBI makes it difficult for a single *in vitro* model to be representative of all facets of the injury response (Enriquez and Bullock, 2004; Raghupathi, 2004). Third, the pro-inflammatory response of NCAM in *in vitro* TBI model still needed to be further investigated and detailed; it would be very informative to compare the cytokine/chemokine profiles between NCAM, microglia from TBI brains, and HMGB1 or LPS-activated microglia to confirm that the NCAM has a cytokine/chemokine profile closer to microglia from TBI brains. Fourth, the comprehensive comparison of metabolic profile between NCAM and TBI microglia would be helpful to further evaluate the *in vitro* model of TBI. We will further determine the metabolic profile of microglia, and validated whether microglial glycolysis plays a key role in controlling microglial activation and mediated secondary neuronal injury in the CCI model in our next study. Fifth, although the excess pro-inflammatory activation of microglia is neurotoxic (Polazzi and Contestabile, 2002), microglia also execute crucial functions toward limiting brain injury and neuro-repair (Jassam et al., 2017). However, this *in vitro* model is suited for investigating the role of activated microglia in mediating neuronal recovery/regeneration. Exploring the important neuroprotective aspects of microglial function is worthy of establishing a new specific *in vitro* model by altering this existing platform.

In summary, this *in vitro* TBI model provides an advanced and highly translational platform for dissecting cellular interactions in the pathologic processes of primary neuronal injury-microglial activation-neuronal degeneration cascade, and elucidating the detailed underlying cellular and molecular insights after TBI.

In conclusion, we newly established, characterized, and applied a microglial activation *in vitro* TBI model for studying neuroinflammation-associated secondary injury mechanisms

after TBI. This *in vitro* model can be used to dissect the effect of damaged neurons on microglial activation, and the specific role of the reactive microglia in mediating neurodegeneration. This *in vitro* model would be a powerful tool to investigate the underlying metabolic and molecular mechanisms which contribute to the microglial proinflammatory activation-derived progressive secondary injury mechanisms following TBI.

References

- Alam A, Thelin EP, Tajsic T, Khan DZ, Khellaf A, Patani R, Helmy A (2020) Cellular infiltration in traumatic brain injury. *J Neuroinflammation* 17:328.
- Bae YH, Joo H, Bae J, Hyeon SJ, Her S, Ko E, Choi HG, Ryu H, Hur EM, Bu Y, Lee BD (2018) Brain injury induces HIF-1 α -dependent transcriptional activation of LRRK2 that exacerbates brain damage. *Cell Death Dis* 9:1125.
- Bernier LP, York EM, MacVicar BA (2020a) Immunometabolism in the brain: how metabolism shapes microglial function. *Trends Neurosci* 43:854–869.
- Bernier LP, York EM, Kamyabi A, Choi HB, Weilinger NL, MacVicar BA (2020b) Microglial metabolic flexibility supports immune surveillance of the brain parenchyma. *Nat Commun* 11:1559.
- Bray CE, Witcher KG, Adekunle-Adegbe D, Ouvia M, Witzel M, Hans E, Tapp ZM, Packer J, Goodman E, Zhao F, Chunchai T, O'Neil S, Chattipakorn SC, Sheridan J, Kokiko-Cochran ON, Askwith C, Godbout JP (2022) Chronic cortical inflammation, cognitive impairment, and immune reactivity associated with diffuse brain injury are ameliorated by forced turnover of microglia. *J Neurosci* 42:4215–4228.
- Cao Y, et al. (2019) PFKFB3-mediated endothelial glycolysis promotes pulmonary hypertension. *Proc Natl Acad Sci USA* 116:13394–13403.
- Cheng C, Wang X, Jiang Y, Li Y, Liao Z, Li W, Yu Z, Whalen MJ, Lok J, Dumont AS, Liu N, Wang X (2021a) Recombinant annexin A2 administration improves neurological outcomes after traumatic brain injury in mice. *Front Pharmacol* 12:708469.
- Cheng J, Zhang R, Xu Z, Ke Y, Sun R, Yang H, Zhang X, Zhen X, Zheng LT (2021b) Early glycolytic reprogramming controls microglial inflammatory activation. *J Neuroinflammation* 18:129.
- Covington NV, Duff MC (2021) Heterogeneity is a hallmark of traumatic brain injury, not a limitation: a new perspective on study design in rehabilitation research. *Am J Speech Lang Pathol* 30:974–985.
- Cox CS Jr (2018) Cellular therapy for traumatic neurological injury. *Pediatr Res* 83:325–332.
- Davalos D, Grutzendler J, Yang G, Kim JV, Zuo Y, Jung S, Littman DR, Dustin ML, Gan WB (2005) ATP mediates rapid microglial response to local brain injury in vivo. *Nat Neurosci* 8:752–758.
- de Haas AH, Boddeke HW, Brouwer N, Biber K (2007) Optimized isolation enables ex vivo analysis of microglia from various central nervous system regions. *Glia* 55:1374–1384.
- Donat CK, Scott G, Gentleman SM, Sastre M (2017) Microglial activation in traumatic brain injury. *Front Aging Neurosci* 9:208.
- Enriquez P, Bullock R (2004) Molecular and cellular mechanisms in the pathophysiology of severe head injury. *Curr Pharm Des* 10:2131–2143.
- Frankowski JC, Tierno A, Pavani S, Cao Q, Lyon DC, Hunt RF (2022) Brain-wide reconstruction of inhibitory circuits after traumatic brain injury. *Nat Commun* 13:3417.
- Gao HM, Zhou H, Zhang F, Wilson BC, Kam W, Hong JS (2011) HMGB1 acts on microglia Mac1 to mediate chronic neuroinflammation that drives progressive neurodegeneration. *J Neurosci* 31:1081–1092.
- Gottlieb A, Toledano-Furman N, Prabhakara KS, Kumar A, Caplan HW, Bedi S, Cox CS Jr, Olson SD (2022) Time dependent analysis of rat microglial surface markers in traumatic brain injury reveals dynamics of distinct cell subpopulations. *Sci Rep* 12:6289.
- Henry RJ, Ritzel RM, Barrett JP, Doran SJ, Jiao Y, Leach JB, Szeto GL, Wu J, Stoica BA, Faden AI, Loane DJ (2020) Microglial depletion with CSF1R inhibitor during chronic phase of experimental traumatic brain injury reduces neurodegeneration and neurological deficits. *J Neurosci* 40:2960–2974.
- Isakharov A, Butler CR (2020) Does delayed microglial ablation alter outcomes after traumatic brain injury? *J Neurosci* 40:8211–8213.

- Jassam YN, Izzy S, Whalen M, McGavern DB, El Khoury J (2017) Neuroimmunology of traumatic brain injury: time for a paradigm shift. *Neuron* 95:1246–1265.
- Kaushal V, Schlichter LC (2008) Mechanisms of microglia-mediated neurotoxicity in a new model of the stroke penumbra. *J Neurosci* 28:2221–2230.
- Kumaria A (2017) In vitro models as a platform to investigate traumatic brain injury. *Altern Lab Anim* 45:201–211.
- Lauterbach MA, Hanke JE, Serefidou M, Mangan MS, Kolbe CC, Hess T, Rothe M, Kaiser R, Hoss F, Gehlen J, Engels G, Kreutzenbeck M, Schmidt SV, Christ A, Imhof A, Hiller K, Latz E (2019) Toll-like receptor signaling rewires macrophage metabolism and promotes histone acetylation via ATP-citrate lyase. *Immunity* 51:997–1011.e1017.
- Lin L, Desai R, Wang X, Lo EH, Xing C (2017) Characteristics of primary rat microglia isolated from mixed cultures using two different methods. *J Neuroinflammation* 14:101.
- Liu N, Yu Z, Xun Y, Shu P, Yue Y, Yuan S, Jiang Y, Huang Z, Yang X, Feng X, Xiang S, Wang X (2018) Amyloid-beta25-35 upregulates endogenous neuroprotectant neuroglobin via NFkappaB activation in vitro. *J Alzheimers Dis* 64:1163–1174.
- Liu N, Han J, Li Y, Jiang Y, Shi SX, Lok J, Whalen M, Dumont AS, Wang X (2021) Recombinant annexin A2 inhibits peripheral leukocyte activation and brain infiltration after traumatic brain injury. *J Neuroinflammation* 18:173.
- Martinez-Reyes I, Chandel NS (2020) Mitochondrial TCA cycle metabolites control physiology and disease. *Nat Commun* 11:102.
- McNair K, Spike R, Guilding C, Prendergast GC, Stone TW, Cobb SR, Morris BJ (2010) A role for RhoB in synaptic plasticity and the regulation of neuronal morphology. *J Neurosci* 30:3508–3517.
- Morrison B 3rd, Elkin BS, Dolle JP, Yarmush ML (2011) In vitro models of traumatic brain injury. *Annu Rev Biomed Eng* 13:91–126.
- Namjoshi DR, Cheng WH, McInnes KA, Martens KM, Carr M, Wilkinson A, Fan J, Robert J, Hayat A, Crompton PA, Wellington CL (2014) Merging pathology with biomechanics using CHIMERA (Closed-Head Impact Model of Engineered Rotational Acceleration): a novel, surgery-free model of traumatic brain injury. *Mol Neurodegener* 9:55.
- Pang Z, Chong J, Zhou G, de Lima Morais DA, Chang L, Barrette M, Gauthier C, Jacques PE, Li S, Xia J (2021) MetaboAnalyst 5.0: narrowing the gap between raw spectra and functional insights. *Nucleic Acids Res* 49:W388–W396.
- Polazzi E, Contestabile A (2002) Reciprocal interactions between microglia and neurons: from survival to neuropathology. *Rev Neurosci* 13:221–242.
- Raghupathi R (2004) Cell death mechanisms following traumatic brain injury. *Brain Pathol* 14:215–222.
- Roozenbeek B, Maas AI, Menon DK (2013) Changing patterns in the epidemiology of traumatic brain injury. *Nat Rev Neurol* 9:231–236.
- Roque PJ, Costa LG (2017) Coculture of neurons and microglia. *Curr Protoc Toxicol* 74:11–24.
- Sakamuri S, Sure VN, Kolli L, Liu N, Evans WR, Sperling JA, Busija DW, Wang X, Lindsey SH, Murfee WL, Mostany R, Katakam PV (2022) Glycolytic and oxidative phosphorylation defects precede the development of senescence in primary human brain microvascular endothelial cells. *Geroscience* 44:1975–1994.
- Salvador E, Burek M, Forster CY (2015) Stretch and/or oxygen glucose deprivation (OGD) in an in vitro traumatic brain injury (TBI) model induces calcium alteration and inflammatory cascade. *Front Cell Neurosci* 9:323.
- Schimmel SJ, Acosta S, Lozano D (2017) Neuroinflammation in traumatic brain injury: a chronic response to an acute injury. *Brain Circ* 3:135–142.
- Shi AC, Rohlwinck U, Scafidi S, Kannan S (2020) Microglial metabolism after pediatric traumatic brain injury: overlooked bystanders or active participants? *Front Neurol* 11:62999.
- Simon DW, McGeachy MJ, Bayir H, Clark RS, Loane DJ, Kochanek PM (2017) The far-reaching scope of neuroinflammation after traumatic brain injury. *Nat Rev Neurol* 13:171–191.
- Simon DW, Aneja RK, Alexander H, Bell MJ, Bayir H, Kochanek PM, Clark RS (2018) Minocycline attenuates high mobility group box 1 translocation, microglial activation, and thalamic neurodegeneration after traumatic brain injury in post-natal day 17 rats. *J Neurotrauma* 35:130–138.
- van Gastel N, Spinelli JB, Sharda A, Schajnovitz A, Baryawno N, Rhee C, Oki T, Grace E, Soled HJ, Milosevic J, Sykes DB, Hsu PP, Vander Heiden MG, Vidoudez C, Trauger SA, Haigis MC, Scadden DT (2020) Induction of a timed metabolic collapse to overcome cancer chemoresistance. *Cell Metab* 32:391–403.e396.
- Wang G, Zhang J, Hu X, Zhang L, Mao L, Jiang X, Liou AK, Leak RK, Gao Y, Chen J (2013) Microglia/macrophage polarization dynamics in white matter after traumatic brain injury. *J Cereb Blood Flow Metab* 33:1864–1874.
- Wang X, Mori T, Jung JC, Fini ME, Lo EH (2002) Secretion of matrix metalloproteinase-2 and -9 after mechanical trauma injury in rat cortical cultures and involvement of MAP kinase. *J Neurotrauma* 19:615–625.
- Weber MD, Frank MG, Tracey KJ, Watkins LR, Maier SF (2015) Stress induces the danger-associated molecular pattern HMGB-1 in the hippocampus of male Sprague Dawley rats: a priming stimulus of microglia and the NLRP3 inflammasome. *J Neurosci* 35:316–324.
- Williams NC, O'Neill LA (2018) A role for the Krebs cycle intermediate citrate in metabolic reprogramming in innate immunity and inflammation. *Front Immunol* 9:141.
- Witcher KG, Bray CE, Chunchai T, Zhao F, O'Neil SM, Gordillo AJ, Campbell WA, McKim DB, Liu X, Dziabis JE, Quan N, Eiferman DS, Fischer AJ, Kokiko-Cochran ON, Askwith C, Godbout JP (2021) Traumatic brain injury causes chronic cortical inflammation and neuronal dysfunction mediated by microglia. *J Neurosci* 41:1597–1616.
- Wofford KL, Loane DJ, Cullen DK (2019) Acute drivers of neuroinflammation in traumatic brain injury. *Neural Regen Res* 14:1481–1489.
- Wohleb ES, Hanke ML, Corona AW, Powell ND, Stiner LM, Bailey MT, Nelson RJ, Godbout JP, Sheridan JF (2011) β -Adrenergic receptor antagonism prevents anxiety-like behavior and microglial reactivity induced by repeated social defeat. *J Neurosci* 31:6277–6288.
- Wu YH, Rosset S, Lee TR, Dragunow M, Park T, Shim V (2021) In vitro models of traumatic brain injury: a systematic review. *J Neurotrauma* 38:2336–2372.
- Xiong Y, Mahmood A, Chopp M (2013) Animal models of traumatic brain injury. *Nat Rev Neurosci* 14:128–142.
- Yang C, Ko B, Hensley CT, Jiang L, Wasti AT, Kim J, Sudderth J, Calvaruso MA, Lumata L, Mitsche M, Rutter J, Merritt ME, DeBerardinis RJ (2014) Glutamine oxidation maintains the TCA cycle and cell survival during impaired mitochondrial pyruvate transport. *Mol Cell* 56:414–424.
- Yang S, Qin C, Hu ZW, Zhou LQ, Yu HH, Chen M, Bosco DB, Wang W, Wu LJ, Tian DS (2021) Microglia reprogram metabolic profiles for phenotype and function changes in central nervous system. *Neurobiol Dis* 152:105290.
- Yu Z, Liu N, Li Y, Xu J, Wang X (2013) Neuroglobin overexpression inhibits oxygen-glucose deprivation-induced mitochondrial permeability transition pore opening in primary cultured mouse cortical neurons. *Neurobiol Dis* 56:95–103.
- Yuan M, Kremer DM, Huang H, Breitkopf SB, Ben-Sahra I, Manning BD, Lyssiotis CA, Asara JM (2019) Ex vivo and in vivo stable isotope labelling of central carbon metabolism and related pathways with analysis by LC-MS/MS. *Nat Protoc* 14:313–330.